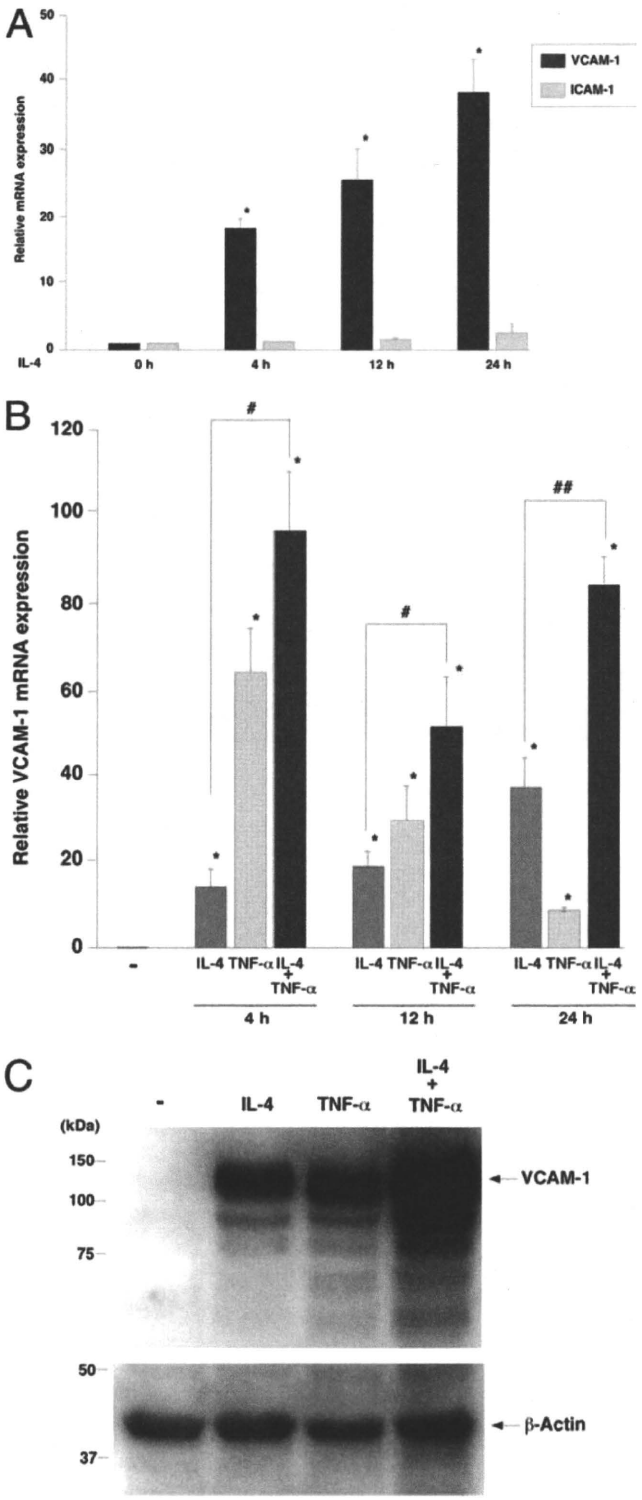

FIG. 1. IL-4-mediated induction of VCAM-1 expression in primary cultured endothelial cells. (A) Confluent HUVECs were serum starved for 16 h and treated with 20 ng/ml IL-4 for the indicated times. Total RNA was harvested and assayed by quantitative real-time PCR for VCAM-1 and ICAM-1 mRNA levels. Data are expressed relative to untreated cells as means ± standard deviations ($n = 4$). *, $P < 0.001$ compared with untreated control. (B) HUVECs were treated with IL-4 and/or TNF-α for the indicated times and then assayed for VCAM-1 mRNA levels using quantitative real-time PCR. Data are expressed relative to untreated cells as means ± standard deviation ($n = 4$). *, $P < 0.01$ compared with untreated cells; #, $P < 0.01$, and ##, $P < 0.05$, compared with IL-4-treated cells at each time point. (C) HUVECs were treated as described above for 24 h. Western blotting was performed using anti-VCAM-1 antibody. The membrane was stripped and reprobed with anti-β-actin antibody as a loading control. Shown are representative data from three independent experiments.

The mechanisms underlying IL-4-mediated induction of VCAM-1 are poorly understood. A previous analysis of the VCAM-1 promoter failed to reveal STAT6 binding sites (16). One study demonstrated that IL-4-dependent increase in VCAM-1 levels is mediated by stabilization of VCAM-1 mRNA (16). A role for reactive oxygen species has also been suggested (23). The goal of the present study was to delineate the molecular basis for IL-4-mediated induction of VCAM-1 expression in endothelial cells. Using a combination of chromatin immunoprecipitation sequencing (ChIP-seq) and functional promoter analyses, we show that IL-4 induction of VCAM-1 is mediated by a STAT6 binding site at kb −16 relative to the transcriptional start site.

MATERIALS AND METHODS

Mice. All experiments were performed with 6- to 8-week-old male C57BL/6 mice (CLEA). Mouse IL-4 (PeproTech) or mouse TNF-α (PeproTech) was dissolved in phosphate-buffered saline (PBS) and injected intravenously (i.v.). All animal studies were approved by the University of Tokyo Institutional Animal Care and Use Committee.

Immunofluorescence studies. Frozen tissue sections (10 μm) were fixed and incubated with a rat monoclonal anti-VCAM-1 antibody (1:50 dilution) (BD Pharmingen) and a goat polyclonal anti-ICAM-2 antibody (8 μg/ml) (R&D Systems) overnight at 4°C. Sections were washed 3 times in PBS and incubated with secondary antibody labeled with Alexa Fluor 594 (for VCAM-1) or Alexa Fluor 488 (for ICAM-2) (1:50 dilution) (Invitrogen) for 1 h at room temperature. The slides were then washed in PBS, mounted in ProLong Gold antifade reagent with DAPI (4′,6-diamidino-2-phenylindole) (Invitrogen), and examined by fluorescence microscopy.

Cell culture. Human umbilical vein endothelial cells (HUVECs) were purchased from Lonza and cultured in EGM-2 medium containing 2% fetal bovine serum (FBS) (Lonza). Cells were used at passages 3 to 4. HUVECs were stimulated with human IL-4 (20 ng/ml; PeproTech) and/or human TNF-α (10 ng/ml; PeproTech). HEK-293 (ATCC CRL-1573) human embryonic kidney cells were cultured in Dulbecco's modified Eagle medium supplemented with 10% FBS. Human U937 cells (JCRB-9021; Japan) were grown in RPMI 1640 medium supplemented with 10% FBS.

Generation of CA-STAT6 adenoviruses. Human STAT6 was cloned by PCR using total RNA from HUVECs and STAT6-specific primers (sequences are shown in Table S1 in the supplemental material). Constitutively active STAT6 (CA-STAT6) was generated by mutating $V_{547}T_{548}$ to $A_{547}A_{548}$ in human STAT6 (5). The cDNA was subcloned into pIRES2-EGFP (Clontech) and then transferred into the pShuttle and Adeno-X DNA (Clontech) by using the Adeno-X adenoviral expression system (Clontech). All cloned constructs were confirmed by restriction enzyme digestions and automated DNA sequencing.

Quantitative real-time PCR. Two micrograms of TRIzol-extracted RNA was reverse transcribed using SuperScript II enzyme and oligo(dT) primer as specified by Invitrogen. Real-time PCR was performed by using the SYBR green PCR reagent according to the manufacturer's instructions (Applied Biosystems). Primer pair DNA sequences are shown in Table S1 in the supplemental material.

Western blot analysis. Endothelial cells were washed with ice-cold PBS, collected with a cell scraper, and lysed with radioimmunoprecipitation assay (RIPA) buffer as described previously (30). The membrane was blocked with Tris-buffered saline-Tween (TBS-T) containing 2% skim milk and incubated with primary antibody against total STAT6 (Santa Cruz Biotechnology), pSTAT6 (Cell Signaling), VCAM-1 (Santa Cruz Biotechnology), lamin A (Sigma), α-tubulin (Sigma), p65 NF-κB (Santa Cruz Biotechnology), or β-actin (Sigma).

Monocyte adhesion assays. Monocyte adhesion to HUVECs was assayed as previously described (30). In brief, confluent HUVECs were infected with an

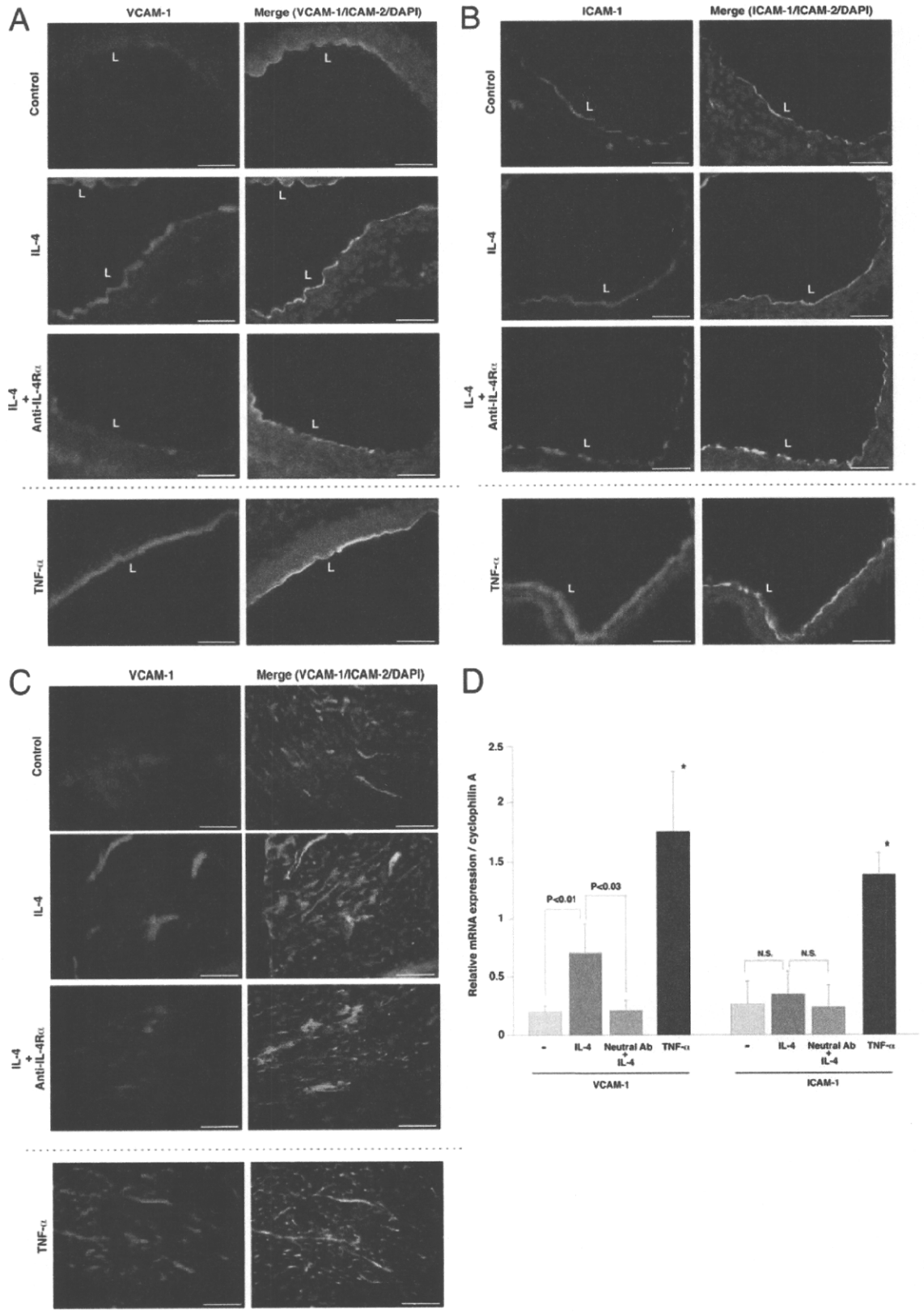

FIG. 2. IL-4-mediated induction of VCAM-1 expression in the intact endothelium. Mice were pretreated with saline (control) or blocking antibody against IL-4Rα and then injected i.v. with control saline, 0.5 mg/kg IL-4, or 0.1 mg/kg TNF-α. Tissues were harvested 6 h later, and cryosections of the aorta (A and B) and heart (C) were collected and stained with anti-VCAM-1 (A and C) or anti-ICAM-1 (B) antibody (left panels, red), ICAM-2 (right panels, green), and DAPI (right panels, blue). Merged images are shown in the right panels. Bar, 50 μm. L, lumen. (D) Total RNA was harvested from hearts and assayed for VCAM-1 or ICAM-1 mRNA levels by quantitative real-time PCR. Ab, antibody. The results show the means and standard deviations of expression levels relative to cyclophilin A from at least four independent sets of mice. *, $P < 0.001$ compared with VCAM-1 or ICAM-1 expression levels with saline treatment. N.S., nonsignificant.

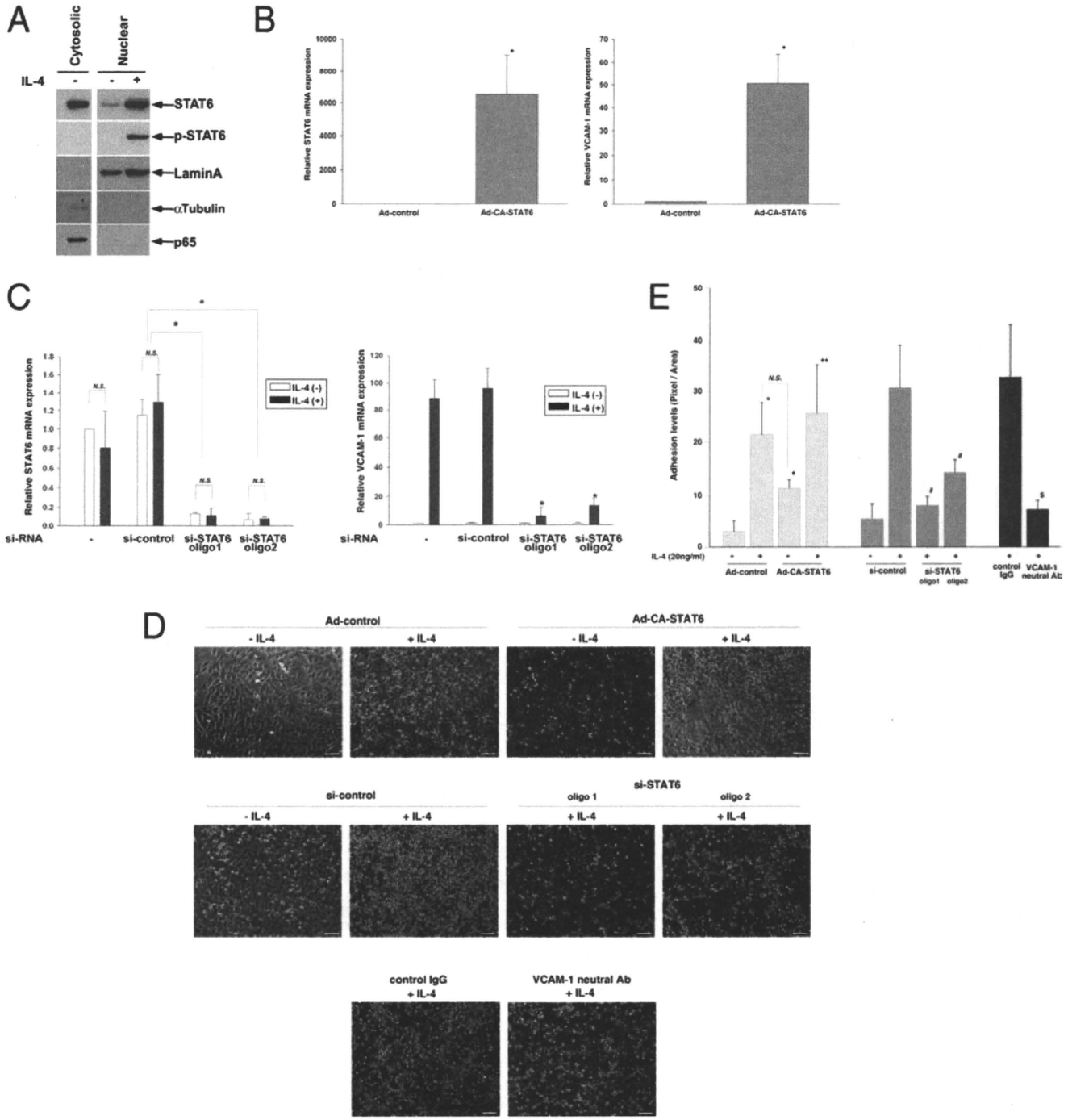

FIG. 3. Role of STAT6 in IL-4-mediated induction of VCAM-1 and monocyte adhesion in primary cultured endothelial cells. (A) HUVECs were treated in the presence or absence of 20 ng/ml IL-4 and then processed for cytosolic and nuclear fractions. Western blot analysis was carried out using antibodies against total STAT6, phospho-STAT6, nuclear lamin A, cytosolic α-tubulin, and p65 NF-κB. (B) HUVECs were treated with Ad-control or Ad-CA-STAT6. STAT6 (left) and VCAM-1 (right) mRNA levels were measured by quantitative real-time PCR. The results show the means and standard deviations of expression levels relative to Ad-control, derived from three independent experiments. *, $P < 0.001$ compared with Ad-control. (C) HUVECs were transfected with si-control or two independent siRNAs against STAT6 (oligo1 or oligo2), serum starved, and then treated with 20 ng/ml IL-4 for 24 h. STAT6 (left) and VCAM-1 (right) mRNA levels were measured by quantitative real-time PCR. The results show the means and standard deviations of expression levels relative to si-control in the absence of IL-4 treatment, derived from at least four independent experiments. *, $P < 0.01$ compared with si-control-treated cells in the presence of IL-4. N.S., nonsignificant. (D and E) U937 monocytic cell adhesion assays were carried out as described in Materials and Methods. HUVECs were infected with Ad-control or Ad-CA-STAT6 or transfected with si-control or si-STAT6, preincubated with control IgG or neutralizing antibody against VCAM-1, treated with 20 ng/ml IL-4 for 24 h, and then washed and incubated with U937 monocytes. The results are representative of four independent optical images from three independent experiments. Bar, 50 μm. Adhesion levels were quantitated (E). *, $P < 0.01$, compared with Ad-control minus IL-4; **, $P = 0.045$ compared with Ad-CA-STAT6 minus IL-4; #, $P < 0.01$ compared with si-control plus IL-4; and $, $P < 0.01$ compared with control IgG.

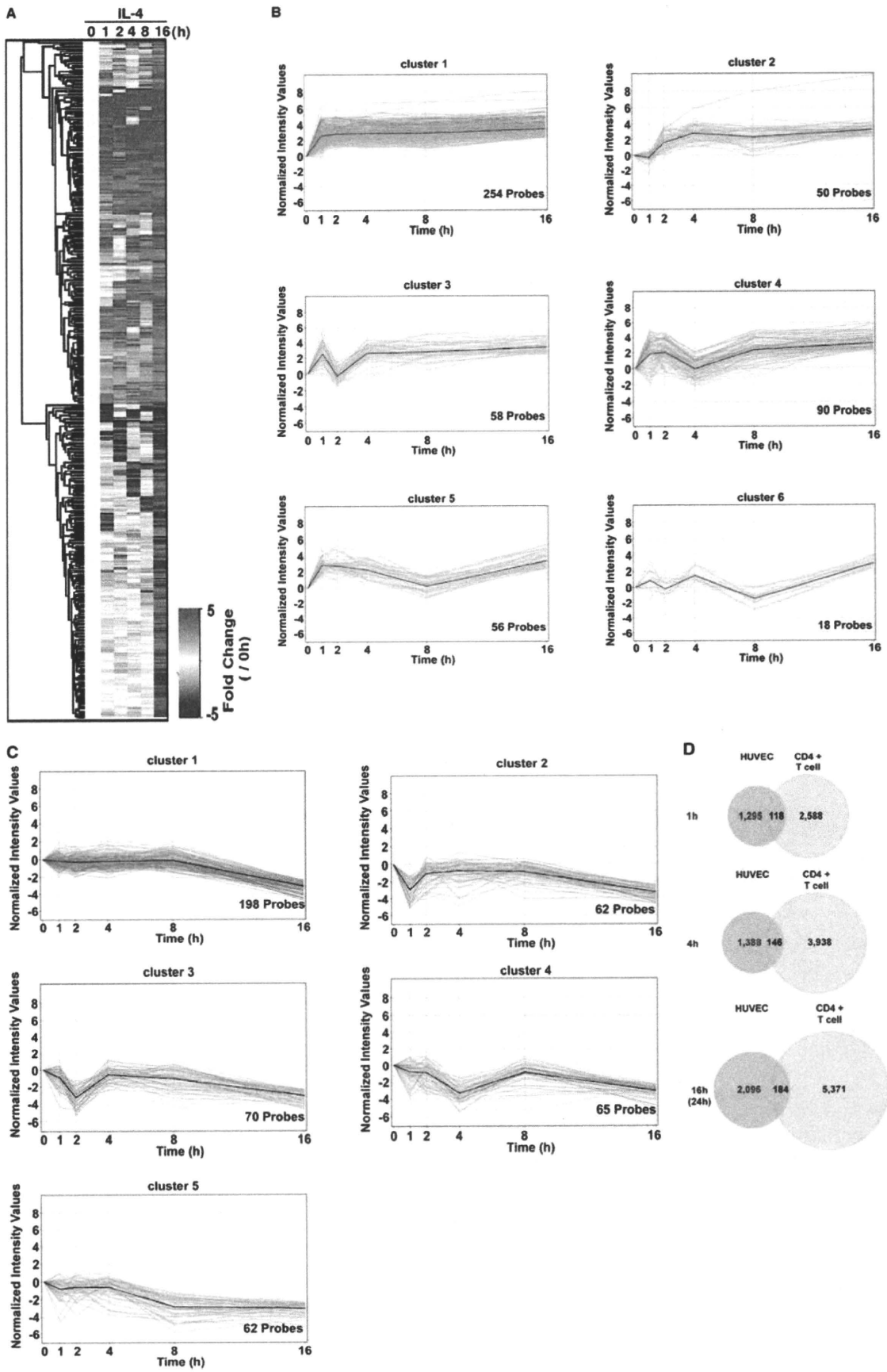
A
IL-4
0 1 2 4 8 16(h)
5
-5
Fold Change
(/ 0h)
B
cluster 1
254 Probes
cluster 2
50 Probes
cluster 3
58 Probes
cluster 4
90 Probes
cluster 5
56 Probes
cluster 6
18 Probes
Normalized Intensity Values
Time (h)
C
cluster 1
198 Probes
cluster 2
62 Probes
cluster 3
70 Probes
cluster 4
65 Probes
cluster 5
62 Probes
D
HUVEC
CD4 +
T cell
1h
1,295
118
2,588
4h
1,388
146
3,938
16h
(24h)
2,096
184
5,371

adenovirus control (Ad-control) or adenovirus expressing constitutively active STAT6 (Ad-CA-STAT6) or transfected with a small interfering RNA (siRNA) control (si-control) or STAT6 siRNA (si-STAT6). Cells were then treated with 20 ng/ml IL-4 for 24 h. PKH-26 (Sigma)-labeled U937 cells were added to a HUVEC-seeded plate. Ninety minutes later, cells were washed and examined by fluorescent microscopy.

Plasmids, transient transfections, and luciferase assays. The construction of VCAM-1-luc (bp −1716 and +119) was previously described (29). The STAT6 binding regions (kbp −16, −11, and +15) were cloned by PCR with genomic DNA from HUVECs and specific primers containing SacI and XhoI sites (shown in Table S1 in the supplemental material). SacI- and XhoI-digested enhancer fragments were subcloned into SacI/XhoI-digested VCAM-1-luc. HUVECs were transiently transfected with plasmid DNA using FuGENE HD reagent (Roche Molecular Biomedicals), and luciferase activity was measured with the dual-luciferase assay kit (Promega) as previously described (31).

DNA microarrays. HUVECs were transfected with either si-control or si-STAT6 (oligo1 or oligo2) for 48 h. Alternatively, HUVECs were infected with Ad-control or Ad-CA-STAT6. RNA was harvested and purified with TRIzol (Invitrogen). Preparation of cRNA and hybridization of probe arrays were performed according to the manufacturer's instructions (Affymetrix). Data were analyzed according to the MIAME rule.

ChIP. HUVECs were cross-linked with 1 mM disuccinimidyl glutarate (Pierce) for 30 min at room temperature, washed once with ice-cold PBS, and cross-linked again using 1% formaldehyde for 10 min at room temperature. Cells were prepared for chromatin immunoprecipitation (ChIP) (data are available at http://www.lsbm.org/MCB_2146207). Antibodies against histone H3 lysine 4 trimethyl (H3K4me3) (ab8580; Abcam), histone H3 lysine 4 monomethyl (H3K4me1) (kindly provided by H. Kimura), p300 (05-257; Upstate), acetylated histone H4 (H4Ac) (06-866; Upstate), and STAT6 (sc-621; Santa Cruz) were added and immunoprecipitated with protein A/G-conjugated magnetic beads (Invitrogen). Prepared DNA was quantified by using Qubit (Invitrogen), and more than 10 ng of DNA was processed for ChIP-seq and ChIP-quantitative PCR (qPCR).

ChIP-seq. All protocols for Illumina/Solexa sequence preparation, sequencing, and quality control are provided by Illumina. A brief summary of the technique and minor protocol modifications are available at http://www.lsbm.org/MCB_2146207.

Statistics. Data are shown as means ± standard deviations (SD). *P* values were calculated by using the two-tailed unpaired Student's *t* test. A *P* value of <0.05 was considered significant.

Accession numbers. Annotation of the probe numbers and targeted sequences are shown on the Affymetrix web page under accession no. GSE 28117. ChIP-seq data are available under accession no. SRA030735.1.

RESULTS

IL-4 induces VCAM-1 but not ICAM-1 expression in cultured endothelial cells. Previous studies have shown that IL-4 induces VCAM-1 expression in cultured endothelial cells (15). Consistent with these data, incubation of human umbilical vein endothelial cells (HUVECs) with 20 ng/ml IL-4 resulted in a time-dependent increase in IL-4 mRNA, as measured by real-time PCR, with peak levels (39.6-fold) occurring at 24 h (Fig. 1A). In contrast, IL-4 did not affect ICAM-1 mRNA expression. Compared with IL-4, TNF-α resulted in an earlier though far greater peak (64.5-fold at 4 h) in VCAM-1 mRNA levels (Fig. 1B). Combined treatment with IL-4 and TNF-α resulted in additive (at 4 and 12 h) and synergistic (at 24 h) induction of VCAM-1 expression (Fig. 1B). In Western blot analyses, treatment of HUVECs for 24 h with IL-4 or TNF-α resulted in comparable induction of VCAM-1 protein levels, while combined treatment with IL-4 and TNF-α resulted in further induction of VCAM-1 (Fig. 1C). Thus, IL-4 results in sustained induction of VCAM-1 expression in cultured endothelial cells.

IL-4 induces VCAM-1 but not ICAM-1 expression in endothelial cells *in vivo*. To determine whether IL-4 induces VCAM-1 expression *in vivo*, mice were injected intravenously (i.v.) with IL-4 (0.5 mg/kg) or an equal volume of saline (control). Aortas and hearts were harvested 6 h later, and cryosections were processed for immunostaining of VCAM-1 or ICAM-1 and the endothelial marker ICAM-2. Compared with the control, IL-4 treatment resulted in marked upregulation of VCAM-1 protein in the aorta, the majority of which colocalized with ICAM-2 in the endothelium (Fig. 2A). This effect was blocked by pretreatment with IL-4 receptor-α blocking antibody. TNF-α (0.1 mg/kg i.v.) injection resulted in a comparable induction of VCAM-1 protein expression in aortic endothelium. In contrast, TNF-α, but not IL-4, also resulted in induction of ICAM-1 in both vascular endothelial cells and smooth muscle cells of the aorta (Fig. 2B).

In the heart, IL-4 treatment resulted in increased VCAM-1 protein expression in the endothelial lining of medium-size blood vessels. In contrast, TNF-α induced VCAM-1 expression both in capillaries and in larger vessels (Fig. 2C). IL-4 treatment had no effect on ICAM-1 levels in the heart (data not shown). To quantitate the effect of systemic IL-4 and TNF-α on VCAM-1 expression, mouse hearts were harvested for RNA and processed for real-time PCR. As shown in Fig. 2D, IL-4 and TNF-α treatment resulted in significant (3.3-fold and 8.5-fold, respectively) increases in VCAM-1 mRNA levels. The effect of IL-4 was blocked (98%) by pretreatment with IL-4 receptor blocking antibody. TNF-α, but not IL-4, induced ICAM-1 mRNA expression in the heart (Fig. 2D). Collectively, these findings suggest that IL-4 results in vascular-bed-specific induction of VCAM-1 in the intact endothelium.

STAT6 is required for IL-4-mediated induction of VCAM-1 in cultured endothelial cells. Previous studies have shown that IL-4 activates STAT6 in endothelial cells (36, 40). Moreover, STAT6 has been implicated in IL-4-mediated induction of P-selectin and eotaxin-3 in endothelial cells (18, 20, 32). As shown in Fig. 3A, incubation of HUVECs with 20 ng/ml IL-4 resulted in tyrosine phosphorylation of STAT6 and translocation of STAT6 from the cytosol to the nucleus (at 60 min). In contrast to TNF-α or thrombin, IL-4 failed to promote nuclear translocation of p65 NF-κB (at 60 min).

To determine whether STAT6 induces VCAM-1 expression, HUVECs were infected with adenovirus expressing constitutively active STAT6 (Ad-CA-STAT6). In the absence of cytokine stimulation, Ad-CA-STAT6 resulted in a 52-fold induction of VCAM-1 mRNA levels (Fig. 3B). In contrast, CA-

FIG. 4. Genome-wide analysis of IL-4-mediated up- or downregulated genes in primary cultured endothelial cells. (A) Heat map representation of IL-4-regulated genes. The color intensity indicates the expression level (upregulated in red and downregulated in blue relative to the median in white). A total of 983 probes demonstrating >5-fold upregulation or downregulation in the presence of IL-4 for 16 h were clustered at indicated time points. (B) Kinetics of IL-4-induced genes (526 probes) using Gene Spring software (Agilent). The bold line indicates the median of all probes in each cluster. (C) Kinetics of IL-4-repressed genes (457 probes) using Gene Spring software. The bold line indicates the median of all probes in each cluster. (D) Venn diagram showing overlap of IL-4-induced genes in HUVECs and $CD4^+$ T cells. Whole probes were selected based on >2-fold induction after IL-4 treatment at 1, 4, and 16 h (HUVECs) or 1, 4, and 24 h (T cells).

STAT6 had no effect on ICAM-1 mRNA expression (data not shown; see Table S2 in the supplemental material). To determine whether endogenous STAT6 plays a role in mediating basal and/or inducible expression of VCAM-1, HUVECs were transfected with two independent siRNAs against STAT6 (oligo1 and oligo2). Each si-STAT6 resulted in >85% reduction of STAT6 and VCAM-1 mRNA in cells treated in the absence or presence of IL-4 (Fig. 3C). Taken together, these findings suggest that VCAM-1 is a STAT6-responsive gene and that IL-4 induces VCAM-1 expression via a STAT6-dependent mechanism.

IL-4-mediated STAT6 activation augments monocyte adhesion to cultured endothelial cells. To determine whether STAT6-mediated induction of VCAM-1 has functional consequences in IL-4-treated endothelial cells, we carried out cell adhesion assays using HUVECs and U937 monocyte cells. IL-4 treatment (20 ng/ml for 24 h) of Ad-control-transfected HUVECs resulted in 7.1-fold increased monocyte adhesion (Fig. 3D and E). In the absence of IL-4 treatment, Ad-CA-STAT6 resulted in a 3.7-fold increase in cell adhesion. Treatment of CA-STAT6-expressing HUVECs with IL-4 resulted in further induction of adhesion, but the absolute levels were comparable with those observed in IL-4-treated Ad-control-infected cells. IL-4 treatment of si-control-treated HUVECs resulted in 5.5-fold increased monocyte adhesion (Fig. 3D and E). This effect was attenuated 73.4% and 55.4% by si-STAT6 oligo1 and oligo2, respectively (Fig. 3D and E). Treatment of HUVECs with neutralizing antibody against VCAM-1 resulted in a comparable reduction (74.6%) of IL-4-mediated monocyte adhesion (Fig. 3D and E). Together, these data suggest that STAT6 plays a critical role in IL-4-mediated VCAM-1-dependent monocyte adhesion to endothelial cells.

Genome-wide survey of IL-4-regulated genes in endothelial cells. IL-4 resulted in the sustained induction of VCAM-1. Our next goal was to determine the extent to which IL-4 induced other genes in the endothelial cells. To that end, we carried out whole-genome expression arrays in HUVECs treated in the absence (0 h) or presence of IL-4 (1, 2, 4, 8, and 16 h). IL-4-regulated genes were collected, as those that were up- or downregulated more than 2-fold via IL-4 treatment at 16 h. Using these criteria, a total of 983 gene probes were identified (Fig. 4A). A total of 526 of these were upregulated at 16 h (Fig. 4A, red), and 457 were downregulated at 16 h (Fig. 4A, blue). The IL-4-induced genes were further divided into 6 clusters according to temporal changes in mRNA expression: (i) induced at all time points, (ii) induced after 2 h, (iii) transiently reduced at 2 h, (iv) transiently reduced at 4 h, (v) transiently reduced at 8 h, and (vi) altered in a fluctuating pattern (Fig. 4B). (The full probe list is shown in Table S2 in the supplemental material.) Those genes that were downregulated at 16 h were divided into five temporal patterns: (i) progressively downregulated, (ii) downregulated at 1 h, (iii) downregulated at 2 h, (iv) downregulated at 4 h, and (v) downregulated at 8 h (Fig. 4C). (The full probe list is shown in Table S2 in the supplemental material.)

In a recent study, genome-wide information was reported for IL-4-regulated genes in $CD4^+$ T cells (9). Thus, we had the opportunity to compare expression patterns in IL-4-treated endothelial cells and T lymphocytes. Only ≈10% of the IL-4-inducible gene probes in HUVECs were also upregulated in $CD4^+$ T cells at similar time points (Fig. 4D). For example, suppressor of cytokine signaling 1 (SOCS1) was commonly upregulated in both cell types. (The full list of commonly induced gene probes is shown in Table S3 in the supplemental material.) However, VCAM-1 was specifically induced in endothelial cells, whereas T-cell receptor was selectively upregulated in T cells. Taken together, these findings suggest that IL-4 signaling in endothelial cells results in temporally diverse cell-type-specific changes in gene expression.

Genome-wide survey of IL-4-mediated STAT6 binding in endothelial cells. We next wished to determine whether IL-4-regulated gene expression correlated with STAT6 binding. To identify genes directly bound by STAT6 in IL-4-treated endothelial cells, we carried out chromatin immunoprecipitation (ChIP) with STAT6 antibody in HUVECs treated in the absence (0 h) or presence of IL-4 (1, 4, and 16 h), followed by ChIP-seq analysis. Nonimmunoprecipitated DNA (input DNA) was used as a negative control to define nonspecific binding. Totals of 12,741,937 (0 h), 13,828,587 (1 h), 14,150,991 (4 h), and 14,816,881 (16 h) nonredundant reads were aligned onto the human genome. In IL-4-treated HUVECs, we identified a total of 10,611 STAT6-occupied peaks (Fig. 5A). A total of 542 of these were present in untreated HUVECs and thus likely represent weak, basal STAT6 binding and/or false-positive binding (Fig. 5A, left). All of the remaining binding regions were induced at 1 h. Half of these bindings (5,709/10,069 regions) were transient (average signal ratio, 15.4), occurring at 1 h but not 4 or 16 h (Fig. 5A, right), whereas the rest were sustained at 4 or 16 h (average signal ratio, 59.7) (calculation data not shown).

Previous studies have demonstrated that STAT proteins bind to a $TTCN_{3-4}GAA$ consensus element (14). A recent report using ChIP-seq in T cells showed that while STAT4 bound to a GAA palindrome with a 3-nucleotide spacer, STAT6 preferentially bound to a GAA palindrome separated by a 4-bp spacer ($TTCN_4GAA$) (45). To determine and compare the binding element(s) in our genome-wide analysis between 1 h and 16 h of IL-4 treatment, we searched the consensus motifs of STAT6-bound regions. Similar to the results in T lymphocytes, our data revealed enrichment for the TTC N_4GAA STAT6 binding site at 16 h (Fig. 5B). Transient STAT6 binding yielded a weaker enrichment score, typically at the 5′-TTC-3′ region in the consensus element. Finally, STAT6 binding at 16 h but not 1 h was associated with coenrichment in other transcription factor binding sites, including NFAT and AP-1 (Fig. 5B).

To determine the location of STAT6 binding sites with IL-4 treatment for 16 h, we divided the human genome into 5 regions relative to the transcriptional start site (TSS) of the genes. As shown in Fig. 5C, 53% of STAT6 binding sites were located between −25 kbp and +10 kbp of the genes. Of these binding sites, 4% were in the proximal promoter region (between −5,000 and +1), while 33% and 1% were located in the introns and exons, respectively. The remaining 47% of STAT6 binding sites were localized to intergenic regions.

Binding of STAT6 to DNA does not necessarily correlate with changes in gene expression. To determine the association between genome-wide STAT6 binding and target gene expression, we compared the results of ChIP-seq with those of DNA microarrays of control and IL-4-treated endothelial cells. We

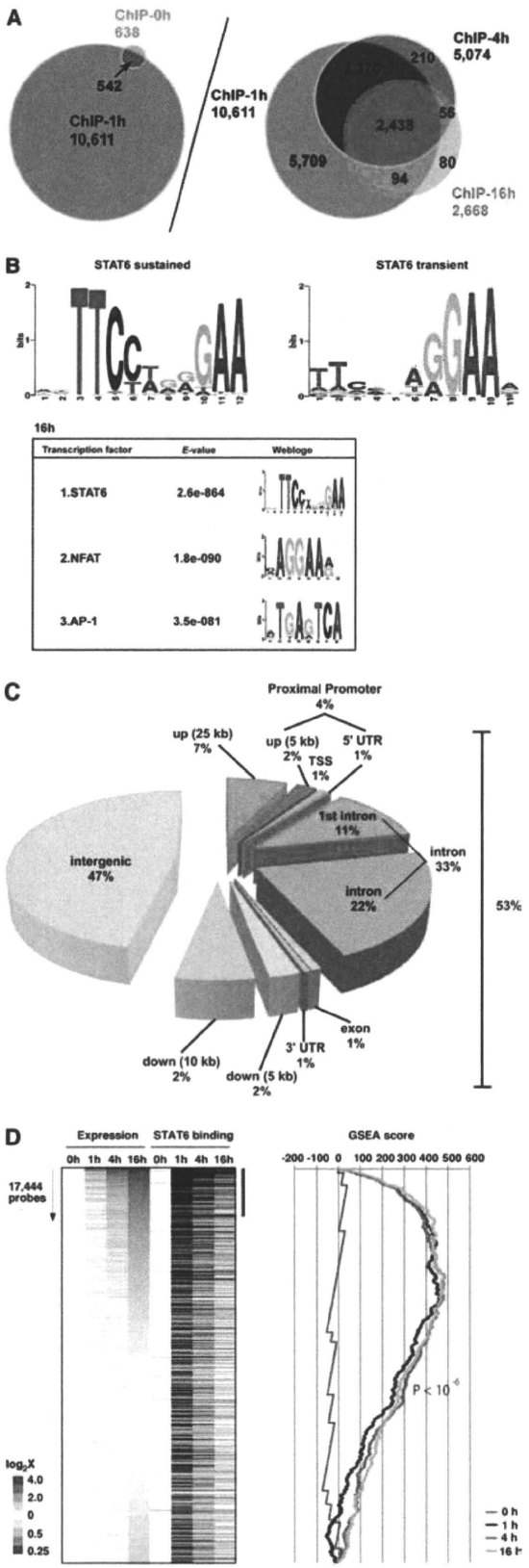

FIG. 5. Genome-wide ChIP-seq analysis of IL-4-mediated STAT6 binding in primary cultured endothelial cells. (A) ChIP-seq analysis was used to survey genome-wide STAT6 binding in HUVECs treated with IL-4 for 0, 1, 4 and 16 h. (B, upper) *De novo* search for STAT6 binding recognition sequence based on sustained or transient binding in HUVECs. (Lower) Second and third enriched motifs calculated by the MEME method. The E-value indicates the probability of *de novo* enriched sequences obtained from ChIP-seq. (C) Distribution of STAT6 binding sites in the proximal promoter (within 5 kb upstream or at the 5′ untranscribed region [UTR] from the transcriptional start site [TSS]), exon, intron, and intergenic regions (defined by regions 25 kb upstream and 10 kb downstream from the TSS). (D) IL-4-responsive genes (based on 17,444 probes [representing ~8,500 genes] in DNA microarrays) at 1, 4, and 16 h, sorted according to the induction ratio at 16 h (left). Genes are aligned with results of ChIP-seq (blue bars indicate STAT6 binding). The vertical black bar indicates a group of highly induced IL-4-responsive genes at 16 h that are enriched in STAT6 binding. A graphic representation of the GSEA enrichment score is shown on the right.

selected microarray gene set probes that exhibited significant expression, as defined by >100 average difference in control HUVECs or HUVECs treated with IL-4 for 1, 4, or 16 h. A total of 17,444 probes (~8,500 genes) met these criteria and were sorted by the log-fold induction/reduction ratio of the expression levels in HUVECs. IL-4 treatment for 1, 4, and 16 h showed a highly significant enrichment score ($P < 10^{-6}$) (Fig. 5D, right). The correlation between IL-4-mediated gene induction and enriched STAT6 binding within the proximal (within 20 kb upstream and downstream of the TSS) was greatest at 16 h of treatment, compared with 1 h and 4 h (Fig. 5D, left). Interestingly, the majority of genes whose expression peaked at 16 h demonstrated STAT6 binding as early as 1 h (see Fig. S1 in the supplemental material). In contrast to IL-4-inducible genes, those genes whose expression was inhibited by IL-4 failed to reveal significant correlation with proximal STAT6 binding (see Fig. S1).

Identification of STAT6-dependent genes in endothelial cells. Subsequently, to determine which IL-4-responsive genes were dependent on STAT6, we carried out duplicate DNA microarrays of control-siRNA- or si-STAT6-transfected HUVECs treated in the absence or presence of IL-4 or HUVECs infected with Ad-CA-STAT6. (The full array data are shown in Table S2 in the supplemental material.) Three gene clusters were identified: (i) IL-4-induced genes stably bound by STAT6 (1, 4, and 16 h) (Fig. 6A, upper one-third, group A), (ii) IL-4-induced genes not stably bound by STAT6 (Fig. 6A, middle one-third, group B), and (iii) IL-4-repressed genes (Fig. 6A, lower one-third, group C). STAT6 knockdown inhibited the effect of IL-4 on 79% of its target genes. The majority of IL-4-inducible STAT6-dependent genes were activated by Ad-CA-STAT6, while many IL-4–STAT6-repressible genes were downregulated by Ad-CA-STAT6 (Fig. 6A). Interestingly, few of the genes that were downregulated by IL-4 demonstrated stable or even transient binding of STAT6. Representative ChIP-seq data from group A are shown for SOCS1, P-selectin, pro-melanin-concentrating hormone (PMCH), and BCL6 (Fig. 6B). In each case, the STAT6 binding region was adjacent to a histone H3 lysine 4 monomethyl (H3K4me1)-positive region (Fig. 6B, blue lines), suggesting that STAT6 binding is associated with transcriptional activation in group A of Fig. 6A. Finally, of those genes that were induced by IL-4 in T cells and HUVECs in a STAT6-dependent manner (at 4 h where data for comparison are available), only 2 were common to both

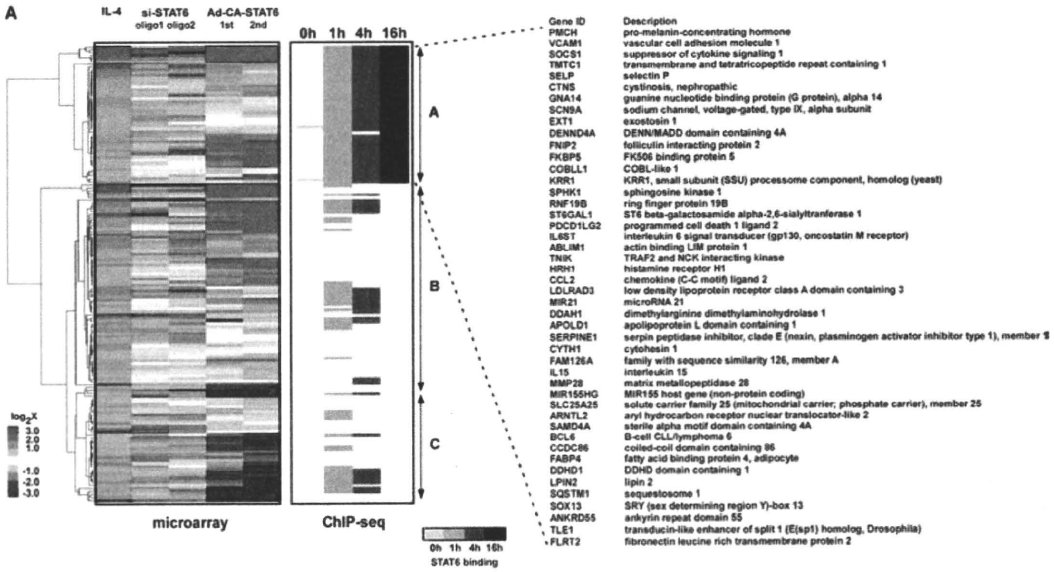
A
IL-4
si-STAT6
oligo1 oligo2
Ad-CA-STAT6
1st 2nd
0h 1h 4h 16h
A
B
C
microarray
ChIP-seq
0h 1h 4h 16h
STAT6 binding
Gene ID Description
PMCH pro-melanin-concentrating hormone
VCAM1 vascular cell adhesion molecule 1
SOCS1 suppressor of cytokine signaling 1
TMTC1 transmembrane and tetratricopeptide repeat containing 1
SELP selectin P
CTNS cystinosis, nephropathic
GNA14 guanine nucleotide binding protein (G protein), alpha 14
SCN9A sodium channel, voltage-gated, type IX, alpha subunit
EXT1 exostosin 1
DENND4A DENN/MADD domain containing 4A
FNIP2 folliculin interacting protein 2
FKBP5 FK506 binding protein 5
COBLL1 COBL-like 1
KRR1 KRR1, small subunit (SSU) processome component, homolog (yeast)
SPHK1 sphingosine kinase 1
RNF19B ring finger protein 19B
ST6GAL1 ST6 beta-galactosamide alpha-2,6-sialyltranferase 1
PDCD1LG2 programmed cell death 1 ligand 2
IL6ST interleukin 6 signal transducer (gp130, oncostatin M receptor)
ABLIM1 actin binding LIM protein 1
TNIK TRAF2 and NCK interacting kinase
HRH1 histamine receptor H1
CCL2 chemokine (C-C motif) ligand 2
LDLRAD3 low density lipoprotein receptor class A domain containing 3
MIR21 microRNA 21
DDAH1 dimethylarginine dimethylaminohydrolase 1
APOLD1 apolipoprotein L domain containing 1
SERPINE1 serpin peptidase inhibitor, clade E (nexin, plasminogen activator inhibitor type 1), member 1
CYTH1 cytohesin 1
FAM126A family with sequence similarity 126, member A
IL15 interleukin 15
MMP28 matrix metallopeptidase 28
MIR155HG MIR155 host gene (non-protein coding)
SLC25A25 solute carrier family 25 (mitochondrial carrier; phosphate carrier), member 25
ARNTL2 aryl hydrocarbon receptor nuclear translocator-like 2
SAMD4A sterile alpha motif domain containing 4A
BCL6 B-cell CLL/lymphoma 6
CCDC86 coiled-coil domain containing 86
FABP4 fatty acid binding protein 4, adipocyte
DDHD1 DDHD domain containing 1
LPIN2 lipin 2
SQSTM1 sequestosome 1
SOX13 SRY (sex determining region Y)-box 13
ANKRD55 ankyrin repeat domain 55
TLE1 transducin-like enhancer of split 1 (E(sp1) homolog, Drosophila)
FLRT2 fibronectin leucine rich transmembrane protein 2

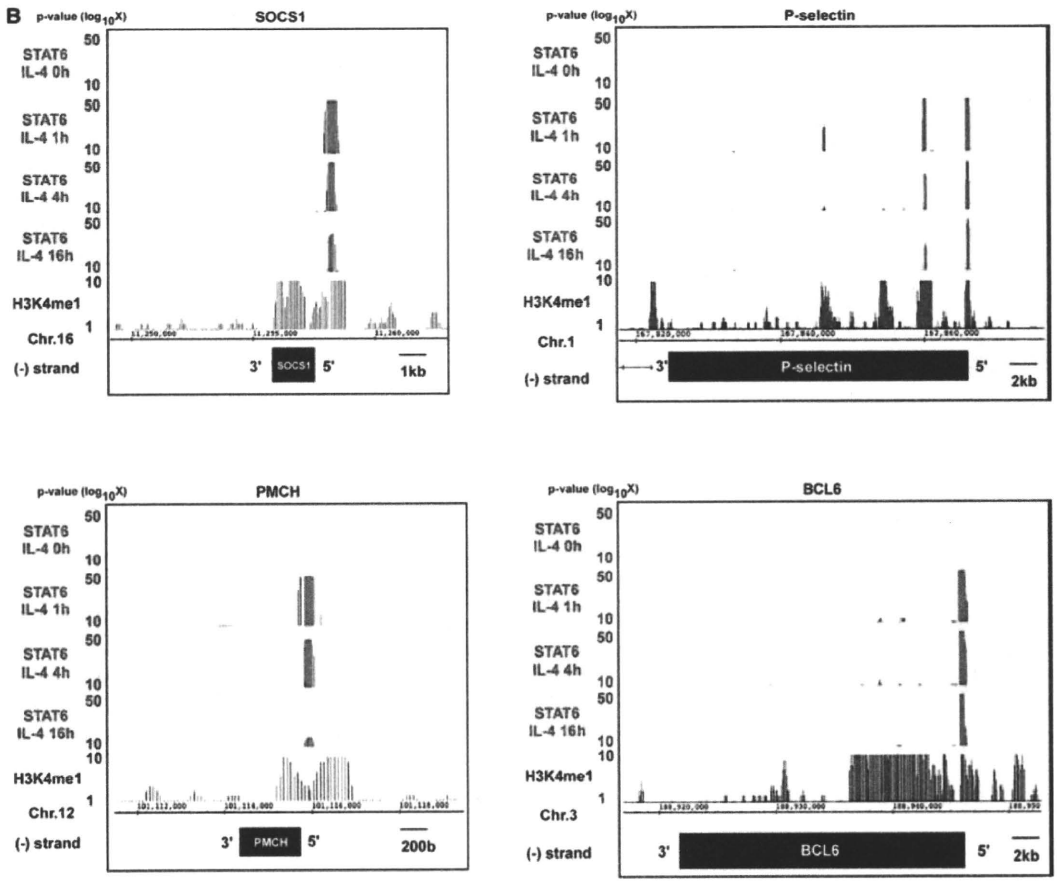
B
p-value (log10X)
SOCS1
STAT6 IL-4 0h
STAT6 IL-4 1h
STAT6 IL-4 4h
STAT6 IL-4 16h
H3K4me1
Chr.16
(-) strand
3'
SOCS1
5'
1kb
P-selectin
Chr.1
P-selectin
2kb
PMCH
Chr.12
PMCH
200b
BCL6
Chr.3
BCL6
2kb

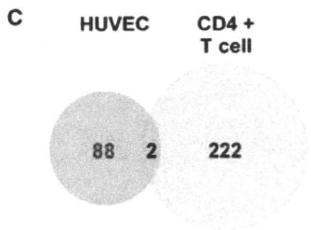
C
HUVEC
CD4 + T cell
88
2
222

cell types (SOCS1 and elongation factor for PolII [ELL]) (Fig. 6C). (The full gene list is shown in Table S4 in the supplemental material.) Taken together, these data suggest that the majority of IL-4-responsive genes are transcriptionally dependent on STAT6. Approximately half of the IL-4-inducible genes are associated with sustained STAT6 binding on the promoter in endothelial cells. Although the IL-4–STAT6 signaling axis is common to endothelial and T cells, the two lineages demonstrate cell-type-specific transcriptional responses.

IL-4-mediated induction of VCAM-1 involves the inducible binding of STAT6 to a distal kb −16 enhancer in the VCAM-1 gene. The VCAM-1 gene was present in the group A into the cluster (Fig. 6A), suggesting that it is a direct STAT6 target gene in IL-4-treated endothelial cells. ChIP-seq revealed three distinct STAT6 binding regions in the VCAM-1 locus (kb −16, −11, and +15, relative to the TSS) (Fig. 7A). Sustained STAT6 binding at 16 h was specifically enriched at the kb −16 region (Fig. 7A). To determine a functional role for the STAT6 binding sites, we carried out luciferase reporter assays in HUVECs with constructs containing a small (minimal) fragment of the human VCAM-1 promoter (between bp −287 and +119) coupled to the STAT6 binding region from kb −16 (244 bp), kb −11 (280 bp), and kb +15 (225 bp) (data not shown). As shown in Fig. 7B, expression of CA-STAT6 failed to induce activity of the minimal VCAM-1 promoter or the minimal promoter coupled to the kb −11 or +15 STAT6 binding region, but significantly increased (4.3-fold) reporter gene expression of the construct containing the core promoter linked to the kb −16 STAT6 binding region [Enhancer (-16)-VCAM-1-luc] (Fig. 7B). Finally, to determine whether IL-4-mediated induction of VCAM-1 requires the kb −16 STAT6 binding region, we carried out reporter analysis with HUVECs treated in the absence or presence of IL-4. IL-4 induced the expression of Enhancer (−16 kb)-VCAM-1-luc (>6-fold) but failed to activate the minimal VCAM-1 core promoter or the promoter coupled to the kb −11 or +15 binding region (Fig. 7C).

The kb −16 enhancer region contains two STAT6 consensus binding motifs (Fig. 7D). To determine whether one or both of these elements are important for STAT6-mediated VCAM-1 promoter activation, we generated Enhancer (−16 kb)-VCAM-1-luc containing single or double point mutations (TT CN_4GAA to $TATN_4GAA$) of the STAT6 binding sites. As shown in Fig. 7D, CA-STAT6-mediated induction of promoter activity was abolished by mutation of the 3′ STAT6 binding site (STAT6 motif 2) or mutation of both sites and was partially inhibited (51.2%) by mutation of the 5′ STAT6 binding site (STAT6 motif 1). Consistent with the results from Ad-CA-STAT6-infected cells, IL-4-mediated activation of Enhancer (−16 kb)-VCAM-1-luc was abolished by mutation of STAT6 motif 2. In contrast, mutation of STAT6 motif 1 had partial (42.9%) blocking on IL-4-mediated VCAM-1 promoter activation (Fig. 7E). Taken together, these findings suggest that IL-4 increases expression of VCAM-1 in endothelial cells by inducing STAT6 binding to a single STAT6 binding element at kb −16.

VCAM-1 enhancer is epigenetically activated with IL-4 treatment. Having established the functional consequences of IL-4-inducible binding of STAT6 to the kb −16 STAT-binding element, we next wished to determine the effect of IL-4 on the epigenetic status of the VCAM-1 locus. To that end, we performed ChIP using antibodies against p300, acetylated histone H4 (H4Ac), H3K4me1, and H3K4me3 in the absence (0 h) or presence (1, 4, and 16 h) of IL-4. The precipitated genome fragments were subjected to the ChIP-qPCR. The MyoD1 promoter region was used as a negative control, since the promoter is silent in control and IL-4-treated endothelial cells. As shown in Fig. 8, IL-4 resulted in enriched binding of H4Ac and H3K4me3 in the proximal promoter region (TSS), consistent with increased capacity for transcriptional activation of the gene. Importantly, IL-4 induced stable binding of p300, H4Ac, and H3K4me1, but not H3K4me3, in the 16-kb region. Taken together, these findings suggest that the endogenous 16-kb STAT6 binding site functions as an IL-4-responsive enhancer. Thus, IL-4 treatment promotes an active chromatin configuration at the kb −16 STAT6 binding region of VCAM-1 in endothelial cells.

DISCUSSION

Endothelial cell activation describes the phenotypic response of endothelial cells to an inflammatory stimulus. When excessive, sustained, and/or uncoupled from local control mechanisms, endothelial cell activation may lead to dysfunction and vascular disease. VCAM-1 is involved in firm adhesion of leukocytes to the apical surface of endothelial cells through interactions with very late antigen 4 (VLA4), which is expressed primarily in lymphocytes and monocytes (reviewed in reference 33). Cross-linking VCAM-1 on the endothelial cell leads to increased cytosolic free calcium, activation of Rac1, and stimulation of reactive oxygen species (33). A pathogenic role for VCAM-1 has been implicated in atherosclerosis (reviewed in references 11 and 33). IL-4 has previously been shown to induce the expression of VCAM-1 in endothelial cells and to play a role in atherosclerotic lesion development. Thus, an understanding of how IL-4 regulates VCAM-1 expression may provide insights into the therapeutic potential of the IL-4–VCAM-1 signaling axis.

We have shown that IL-4 induces VCAM-1 mRNA expression in cultured endothelial cells and in the intact endothelium of mice. The *in vitro* findings are consistent with previously published data, while the observation that systemic adminis-

FIG. 6. Genome-wide analysis of STAT6-regulated genes in primary cultured endothelial cells. (A) Combined representation of microarrays and ChIP-seq results. Array genes were selected by the criteria with more than 2-fold up-or downregulated via IL-4 and were aligned with the results from ChIP-seq (middle column). (B) Representative ChIP-seq data (genome browser view) from SOCS1, P-selectin, PMCH, and BCL6. STAT6 binding signals are shown in red. H3K4me1 signals are shown in blue. Chr.16, chromosome 16. (C) Venn diagram showing the STAT6-dependent IL-4-inducible genes in HUVECs and $CD4^+$T cells. Each number indicates the gene volume, which was induced via IL-4 and bound by STAT6 within the region from kb −20 upstream promoter, TSS, 5′ UTR, or 1st intron.

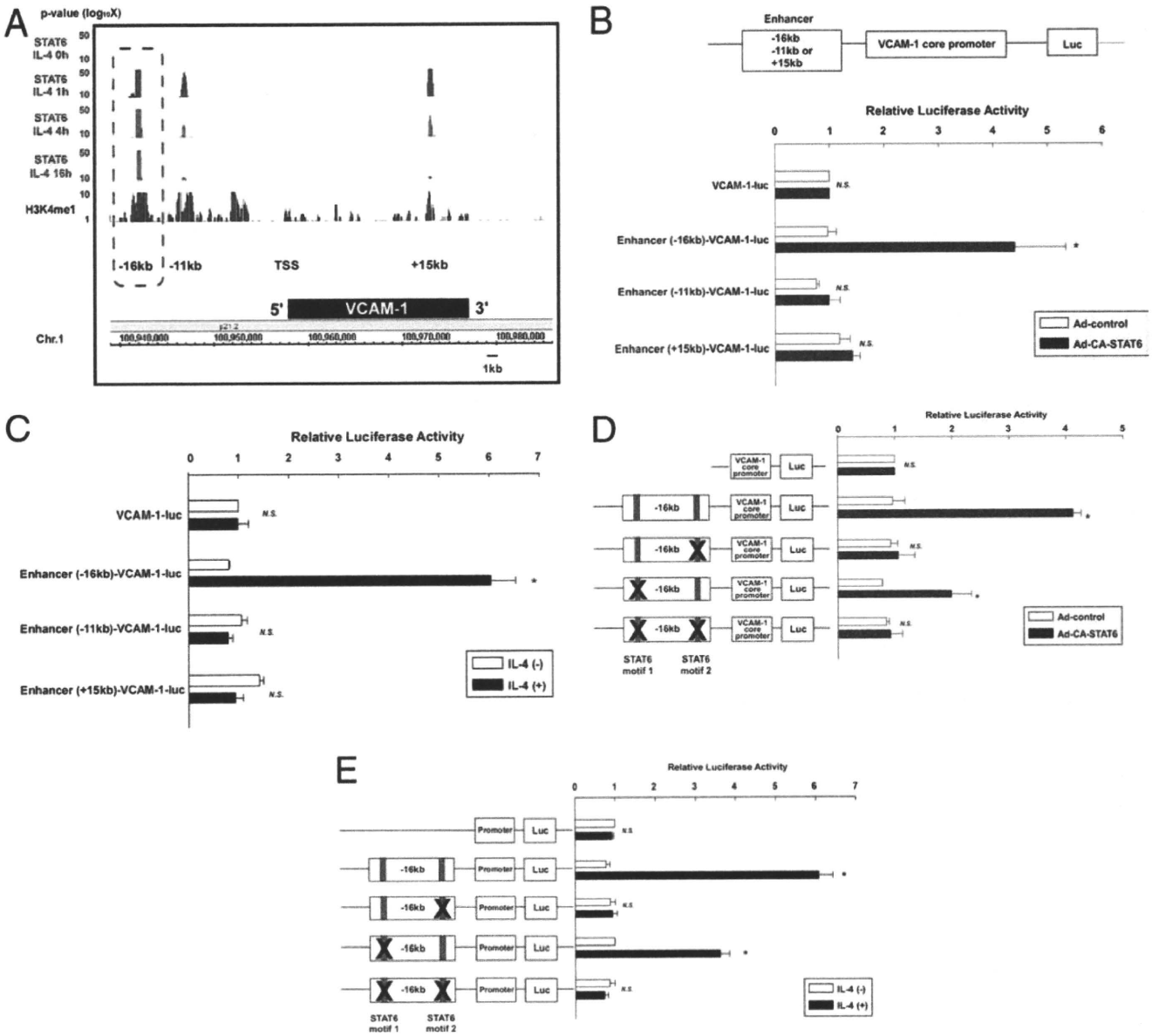

FIG. 7. Identification of the STAT6-bound VCAM-1 enhancer. (A) ChIP-seq data in the VCAM-1 locus with the genome browser view. STAT6 binding signals are shown in red. H3K4me1 signals are shown in blue. The box (dashed red line) indicates the H3K4me1-positive region associated with stable binding of STAT6. Chr.1, chromosome 1. (B, upper) Schematic representation of the luciferase constructs. (Lower) HUVECs were transiently transfected with Enhancer-VCAM-1-luc, serum starved for 16 h, incubated with Ad-control or Ad-CA-STAT6 for 24 h, and then assayed for luciferase activity. The results show the mean ± standard deviations of luciferase light units (relative to VCAM-1-luc- and Ad-control-transfected cells) obtained in triplicate from at least 3 independent experiments. *, $P < 0.01$ compared with Ad-control-transfected cells. N.S., nonsignificant. (C) HUVECs were transiently transfected with VCAM-1-luc or VCAM-1-luc containing the enhancer, serum starved for 16 h, and incubated with IL-4 for 24 h. The results show the mean ± standard deviation of luciferase light units (relative to VCAM-1-luc in the absence of IL-4 treatment) obtained in triplicate from at least 3 independent experiments. *, $P < 0.01$ compared without IL-4 treatment. (D) HUVECs were transiently transfected with VCAM-1-luc, wild-type Enhancer (−16-kb)-VCAM-1-luc, or (Enhancer −16-kb)-VCAM-1-luc containing a point mutation of one or both STAT6 binding elements. Cells were assayed as described above. The results show the mean ± standard deviation of luciferase light units (relative to VCAM-1-luc- and Ad-control-transfected cells) obtained in triplicate from at least 3 independent experiments. *, $P < 0.01$, compared with Ad-control-transfected cells. (E) HUVECs were transiently transfected with plasmids, serum starved, and incubated with IL-4 for 24 h. The results show the mean ± standard deviation of luciferase light units (relative to VCAM-1-luc-transfected cells in the absence of IL-4 treatment) obtained in triplicate from at least 3 independent experiments. *, $P < 0.05$ compared with IL-4-nontreated cells.

tration of IL-4 induces VCAM-1 expression *in vivo* is novel. We cannot rule out the possibility that IL-4-mediated upregulation of VCAM-1 in the endothelium occurs indirectly via IL-4 signaling in another cell type. This limitation notwithstanding, the data provide strong support for VCAM-1 as an IL-4-responsive gene in endothelial cells.

The mechanisms underlying IL-4-mediated induction of VCAM-1 have remained elusive. Previous studies have failed

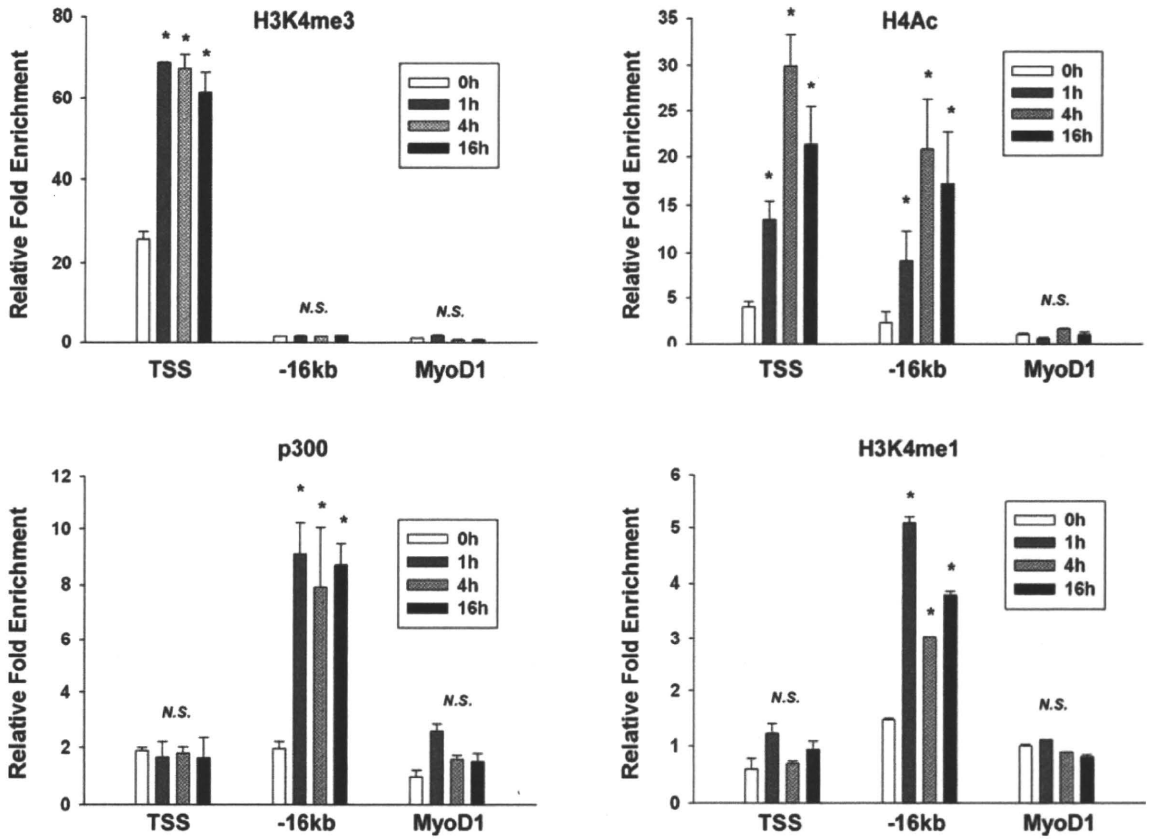

FIG. 8. IL-4-mediated epigenetic modification of the kb −16 VCAM-1 enhancer. HUVECs were treated in the absence (0 h) or presence (1, 4, and 16 h) of IL-4, formalin fixed, and processed for immunoprecipitation of H4Ac, H3K4me3, p300, and H3K4me1. Precipitated genomic DNA was subjected to quantitative real-time PCR using primers specific to the VCAM-1 TSS, the kb −16 VCAM-1 enhancer, and the MyoD1 promoter. Shown is the ChIP enrichment level (mean ± standard deviation) relative to the ChIP-PCR value from the MyoD1 promoter without IL-4 (negative control). *, $P < 0.05$ compared to the same condition without IL-4 treatment. N.S., nonsignificant.

to identify STAT6 binding sites on the VCAM-1 promoter. In the present study, several lines of evidence point to STAT6 as a key regulator of IL-4-inducible VCAM-1 expression. First, IL-4 treatment resulted in increased phosphorylation and nuclear translocation of STAT6. Second, constitutively active STAT6 induced the expression of VCAM-1. Third, IL-4-mediated induction of VCAM-1 was inhibited by si-STAT6. Fourth, ChIP-seq revealed IL-4-inducible binding of STAT6 to several regions of the VCAM-1 gene (at kb −16, −11, and +15). Fifth, in transient transfection assays, a STAT6 binding site 16 kb upstream of the transcriptional start site was found to mediate IL-4 induction of VCAM-1. (This region alone contains consensus STAT6 binding sequences [data are available at http://www.lsbm.org/MCB_2146207].) Finally, IL-4 induced accessible epigenetic marks in the 16-kb region (H3K4me1, H4Ac, and p300), consistent with an enhancing role of the STAT6 binding site at the level of the endogenous gene. Thus, contrary to previous reports, IL-4 does indeed induce VCAM-1 expression by a STAT6-dependent mechanism.

In contrast to the findings with VCAM-1, the IL-4–STAT6 signaling pathway failed to induce ICAM-1 expression *in vitro* and *in vivo*. These data add further evidence for the differential regulation of VCAM-1 and ICAM-1. For example, TNF-α and thrombin induce the expression of VCAM-1 via a GATA- and NF-κB-dependent mechanism, whereas induction of ICAM-1 occurs through NF-κB alone (28). We have shown that histone deacetylase (HDAC) inhibitors attenuate TNF-α-mediated induction of VCAM-1, but not ICAM-1 (19). Finally, FOXO1 has been implicated in VEGF stimulation of VCAM-1 alone (1). Taken together, these findings suggest that VCAM-1 is governed by a more complex repertoire of signaling pathways and transcription factors.

In addition to providing insights into the transcriptional regulation of VCAM-1, the genome-wide approaches used in the present study are the first to reveal the kinetics of IL-4-regulated genes and the time-dependent landscape of transcription factor binding of STAT6 in control and IL-4-treated endothelial cells. By combining DNA microarrays and ChIP-seq, we demonstrated that the majority (79%) of IL-4-responsive genes are STAT6 dependent, as defined by a reversal of the IL-4 effect in STAT6-deficient cells. In addition, IL-4 induction of many of these genes was associated with direct STAT6 binding to their promoter. Importantly, there was little overlap in IL-4-inducible STAT6-dependent genes between endothelial cells and T cells. Collectively, these findings strongly support a predominant cell-type-specific role for STAT6 in mediating IL-4 signal transduction in endothelial cells.

ChIP-seq with STAT6 demonstrated that more than 10,000 independent regions were rapidly occupied by STAT6 at 1 h. In many cases, binding was transient (absent at 4 h and 16 h). However, most genes that were induced at 16 h were already bound by STAT6 at an earlier time point. Thus, in some cases, STAT6 binding may be spurious, while in other cases, STAT6 binding may alter the chromatin microenvironment in such a way as to prime the gene for subsequent IL-4 activation. The enrichment calculation from our ChIP-seq data revealed that stable, but not transient binding of STAT6 occurred at the $TTCN_4GAA$ consensus sequence. Interestingly, stably (at 16 h) but not transiently (at 1 h) bound STAT6 genes demonstrated coenrichment in other transcription factor binding motifs, including NFAT and AP-1 (Fig. 5B). Thus, the stability of STAT6 binding may depend not only on the sequence of the STAT6 consensus motif, but also on an association of STAT6 with other transcription factors.

The use of ChIP-seq has proven useful in unveiling the histone code on a genome-wide scale. For example, a previous report on T cells demonstrated that STAT6 had a predominant role in antagonizing repressive marks on the genome (45). In the present study, we have shown that STAT6 binding to several target genes occurs at sites where epigenetic marks are permissive for transcriptional activation. Further studies are required to determine the extent to which STAT6 binding in endothelial cells causes changes in DNA methylation and the histone code.

In summary, we have employed complementary genome-wide approaches to delineate IL-4-responsive genes whose expression is associated with inducible binding of STAT6 in endothelial cells. The emerging picture is one in which IL-4 promotes rapid and sustained binding of STAT6 to a broad set of target genes. Importantly, our strategy led to the identification of a novel functional kb −16 STAT6 binding site in the VCAM-1 gene. Given the critical role of VCAM-1 in endothelial cell activation and dysfunction, the discovery of new transcriptional control elements may provide a foundation for targeted therapies in vascular disease.

ACKNOWLEDGMENTS

This study was supported by the Leading-Edge Research Promotion Fund from Japan Society for the Promotion of Science (to T.M.), in part supported by a Grant-in-Aid for Scientific Research on Innovative Areas from the Ministry of Education, Culture, Sports, Science, and Technology in Japan (to T.M.), and in part supported by Mochida Memorial and Sankyo Science Foundation in Japan (to T.M.). This study was also in part supported by NIH grants HL082927 and HL076540 (to W.C.A.).

We are grateful to H. Kimura (Osaka University, Japan) for providing the monoclonal antibody against H3K4me1. We thank Akashi Izumi and Mai Miura (RCAST in the University of Tokyo) and Yuki Takagi (Tomy Digital Biology, Inc., Japan) for technical assistance.

REFERENCES

1. **Abid, M. R., et al.** 2006. A novel class of vascular endothelial growth factor-responsive genes that require forkhead activity for expression. J. Biol. Chem. **281:**35544–35553.
2. **Ahmad, M., P. Theofanidis, and R. M. Medford.** 1998. Role of activating protein-1 in the regulation of the vascular cell adhesion molecule-1 gene expression by tumor necrosis factor-alpha. J. Biol. Chem. **273:**4616–4621.
3. **Bennett, B. L., R. Cruz, R. G. Lacson, and A. M. Manning.** 1997. Interleukin-4 suppression of tumor necrosis factor alpha-stimulated E-selectin gene transcription is mediated by STAT6 antagonism of NF-kappaB. J. Biol. Chem. **272:**10212–10219.
4. **Bochner, B. S., D. A. Klunk, S. A. Sterbinsky, R. L. Coffman, and R. P. Schleimer.** 1995. IL-13 selectively induces vascular cell adhesion molecule-1 expression in human endothelial cells. J. Immunol. **154:**799–803.
5. **Bruns, H. A., U. Schindler, and M. H. Kaplan.** 2003. Expression of a constitutively active Stat6 in vivo alters lymphocyte homeostasis with distinct effects in T and B cells. J. Immunol. **170:**3478–3487.
6. **Chapoval, S., P. Dasgupta, N. J. Dorsey, and A. D. Keegan.** Regulation of the T helper cell type 2 (Th2)/T regulatory cell (Treg) balance by IL-4 and STAT6. J. Leukoc. Biol. **87:**1011–1018.
7. **de la Paz, N. G., S. Simeonidis, C. Leo, D. W. Rose, and T. Collins.** 2007. Regulation of NF-kappaB-dependent gene expression by the POU domain transcription factor Oct-1. J. Biol. Chem. **282:**8424–8434.
8. **Doucet, C., et al.** 1998. Interleukin (IL) 4 and IL-13 act on human lung fibroblasts. Implication in asthma. J. Clin. Invest. **101:**2129–2139.
9. **Elo, L. L., et al.** 2010. Genome-wide profiling of interleukin-4 and STAT6 transcription factor regulation of human Th2 cell programming. Immunity **32:**852–862.
10. **Fukushi, J., M. Ono, W. Morikawa, Y. Iwamoto, and M. Kuwano.** 2000. The activity of soluble VCAM-1 in angiogenesis stimulated by IL-4 and IL-13. J. Immunol. **165:**2818–2823.
11. **Galkina, E., and K. Ley.** 2007. Vascular adhesion molecules in atherosclerosis. Arterioscler. Thromb. Vasc. Biol. **27:**2292–2301.
12. **Hamik, A., et al.** 2007. Kruppel-like factor 4 regulates endothelial inflammation. J. Biol. Chem. **282:**13769–13779.
13. **Hosking, B. M., S. C. Wang, M. Downes, P. Koopman, and G. E. Muscat.** 2004. The VCAM-1 gene that encodes the vascular cell adhesion molecule is a target of the Sry-related high mobility group box gene, Sox18. J. Biol. Chem. **279:**5314–5322.
14. **Hou, J., et al.** 1994. An interleukin-4-induced transcription factor: IL-4 Stat. Science **265:**1701–1706.
15. **Huang, H., A. Lavoie-Lamoureux, K. Moran, and J. P. Lavoie.** 2007. IL-4 stimulates the expression of CXCL-8, E-selectin, VEGF, and inducible nitric oxide synthase mRNA by equine pulmonary artery endothelial cells. Am. J. Physiol. Lung Cell. Mol. Physiol. **292:**L1147–L1154.
16. **Iademarco, M. F., J. L. Barks, and D. C. Dean.** 1995. Regulation of vascular cell adhesion molecule-1 expression by IL-4 and TNF-alpha in cultured endothelial cells. J. Clin. Invest. **95:**264–271.
17. **Iademarco, M. F., J. J. McQuillan, G. D. Rosen, and D. C. Dean.** 1992. Characterization of the promoter for vascular cell adhesion molecule-1 (VCAM-1). J. Biol. Chem. **267:**16323–16329.
18. **Inomata, M., T. Into, M. Nakashima, T. Noguchi, and K. Matsushita.** 2009. IL-4 alters expression patterns of storage components of vascular endothelial cell-specific granules through STAT6- and SOCS-1-dependent mechanisms. Mol. Immunol. **46:**2080–2089.
19. **Inoue, K., et al.** 2006. Histone deacetylase inhibitor reduces monocyte adhesion to endothelium through the suppression of vascular cell adhesion molecule-1 expression. Arterioscler. Thromb. Vasc. Biol. **26:**2652–2659.
20. **Khew-Goodall, Y., C. Wadham, B. N. Stein, J. R. Gamble, and M. A. Vadas.** 1999. Stat6 activation is essential for interleukin-4 induction of P-selectin transcription in human umbilical vein endothelial cells. Arterioscler. Thromb. Vasc. Biol. **19:**1421–1429.
21. **Kleemann, R., S. Zadelaar, and T. Kooistra.** 2008. Cytokines and atherosclerosis: a comprehensive review of studies in mice. Cardiovasc. Res. **79:** 360–376.
22. **Kuperman, D. A., and R. P. Schleimer.** 2008. Interleukin-4, interleukin-13, signal transducer and activator of transcription factor 6, and allergic asthma. Curr. Mol. Med. **8:**384–392.
23. **Lee, Y. W., H. Kuhn, B. Hennig, A. S. Neish, and M. Toborek.** 2001. IL-4-induced oxidative stress upregulates VCAM-1 gene expression in human endothelial cells. J. Mol. Cell Cardiol. **33:**83–94.
24. **Lee, Y. W., et al.** 2001. Interleukin 4 induces transcription of the 15-lipoxygenase I gene in human endothelial cells. J. Lipid Res. **42:**783–791.
25. **Lee, Y. W., W. H. Lee, and P. H. Kim.** 2010. Oxidative mechanisms of IL-4-induced IL-6 expression in vascular endothelium. Cytokine **49:**73–79.
26. **Masinovsky, B., D. Urdal, and W. M. Gallatin.** 1990. IL-4 acts synergistically with IL-1 beta to promote lymphocyte adhesion to microvascular endothelium by induction of vascular cell adhesion molecule-1. J. Immunol. **145:** 2886–2895.
27. **Mikita, T., D. Campbell, P. Wu, K. Williamson, and U. Schindler.** 1996. Requirements for interleukin-4-induced gene expression and functional characterization of Stat6. Mol. Cell. Biol. **16:**5811–5820.
28. **Minami, T., et al.** 2003. Thrombin stimulation of vascular adhesion molecule-1 in endothelial cells is mediated by protein kinase C (PKC)-delta-NF-kappa B and PKC-zeta-GATA signaling pathways. J. Biol. Chem. **278:**6976–6984.
29. **Minami, T., and W. C. Aird.** 2001. Thrombin stimulation of the vascular cell adhesion molecule-1 promoter in endothelial cells is mediated by tandem nuclear factor-kappa B and GATA motifs. J. Biol. Chem. **276:**47632–47641.
30. **Minami, T., M. Miura, W. C. Aird, and T. Kodama.** 2006. Thrombin-induced autoinhibitory factor, Down syndrome critical region-1, attenuates NFAT-dependent vascular cell adhesion molecule-1 expression and inflammation in the endothelium. J. Biol. Chem. **281:**20503–20520.
31. **Minami, T., R. D. Rosenberg, and W. C. Aird.** 2001. Transforming growth

factor-beta 1-mediated inhibition of the flk-1/KDR gene is mediated by a 5′-untranslated region palindromic GATA site. J. Biol. Chem. **276:**5395–5402.
32. **Miyazaki, Y., T. Satoh, K. Nishioka, and H. Yokozeki.** 2006. STAT-6-mediated control of P-selectin by substance P and interleukin-4 in human dermal endothelial cells. Am. J. Pathol. **169:**697–707.
33. **Muller, W. A.** 2009. Mechanisms of transendothelial migration of leukocytes. Circ. Res. **105:**223–230.
34. **Neish, A. S., L. M. Khachigian, A. Park, V. R. Baichwal, and T. Collins.** 1995. Sp1 is a component of the cytokine-inducible enhancer in the promoter of vascular cell adhesion molecule-1. J. Biol. Chem. **270:**28903–28909.
35. **Neish, A. S., et al.** 1995. Endothelial interferon regulatory factor 1 cooperates with NF-kappa B as a transcriptional activator of vascular cell adhesion molecule 1. Mol. Cell. Biol. **15:**2558–2569.
36. **Palmer-Crocker, R. L., C. C. Hughes, and J. S. Pober.** 1996. IL-4 and IL-13 activate the JAK2 tyrosine kinase and Stat6 in cultured human vascular endothelial cells through a common pathway that does not involve the gamma c chain. J. Clin. Invest. **98:**604–609.
37. **Palmer-Crocker, R. L., and J. S. Pober.** 1995. IL-4 induction of VCAM-1 on endothelial cells involves activation of a protein tyrosine kinase. J. Immunol. **154:**2838–2845.
38. **Paul, W. E.** 1991. Interleukin-4: a prototypic immunoregulatory lymphokine. Blood **77:**1859–1870.
39. **Rollins, B. J., and J. S. Pober.** 1991. Interleukin-4 induces the synthesis and secretion of MCP-1/JE by human endothelial cells. Am. J. Pathol. **138:**1315–1319.
40. **Schnyder, B., et al.** 2002. Phytochemical inhibition of interleukin-4-activated Stat6 and expression of VCAM-1. Biochem. Biophys. Res. Commun. **292:**841–847.
41. **Stein, N. C., et al.** 2008. Interleukin-4 and interleukin-13 stimulate the osteoclast inhibitor osteoprotegerin by human endothelial cells through the STAT6 pathway. J. Bone Miner. Res. **23:**750–758.
42. **Street, N. E., and T. R. Mosmann.** 1990. IL4 and IL5: the role of two multifunctional cytokines and their place in the network of cytokine interactions. Biotherapy **2:**347–362.
43. **Thornhill, M. H., and D. O. Haskard.** 1990. IL-4 regulates endothelial cell activation by IL-1, tumor necrosis factor, or IFN-gamma. J. Immunol. **145:**865–872.
44. **Umetani, M., et al.** 2001. Function of GATA transcription factors in induction of endothelial vascular cell adhesion molecule-1 by tumor necrosis factor-alpha. Arterioscler. Thromb. Vasc. Biol. **21:**917–922.
45. **Wei, L., et al.** 2010. Discrete roles of STAT4 and STAT6 transcription factors in tuning epigenetic modifications and transcription during T helper cell differentiation. Immunity **32:**840–851.
46. **Wojta, J., et al.** 1993. Interleukin-4 stimulates expression of urokinase-type-plasminogen activator in cultured human foreskin microvascular endothelial cells. Blood **81:**3285–3292.
47. **Yao, L., J. Pan, H. Setiadi, K. D. Patel, and R. P. McEver.** 1996. Interleukin 4 or oncostatin M induces a prolonged increase in P-selectin mRNA and protein in human endothelial cells. J. Exp. Med. **184:**81–92.

blood

2010 115: 2520-2532
Prepublished online November 23, 2009;
doi:10.1182/blood-2009-07-233478

Vascular endothelial growth factor activation of endothelial cells is mediated by early growth response-3

Jun-ichi Suehiro, Takao Hamakubo, Tatsuhiko Kodama, William C. Aird and Takashi Minami

Blood (print ISSN 0006-4971, online ISSN 1528-0020), is published weekly by the American Society of Hematology, 2021 L St, NW, Suite 900, Washington DC 20036.

Vascular endothelial growth factor activation of endothelial cells is mediated by early growth response-3

Jun-ichi Suehiro,[1] Takao Hamakubo,[1] Tatsuhiko Kodama,[1,2] William C. Aird,[3] and Takashi Minami[1,2]

[1]Research Center for Advanced Science and Technology, The University of Tokyo, Tokyo, Japan; [2]Translational Systems Biology and Medicine Initiative (TSBMI), The University of Tokyo, Tokyo, Japan; and [3]Department of Molecular and Vascular Medicine, Beth Israel Deaconess Medical Center/Harvard Medical School, Boston, MA

Endothelial cell activation and dysfunction underlie many vascular disorders, including atherosclerosis, tumor growth, and sepsis. Endothelial cell activation, in turn, is mediated primarily at the level of gene transcription. Here, we show that in response to several activation agonists, including vascular endothelial growth factor (VEGF), tumor necrosis factor-α, and thrombin, endothelial cells demonstrate rapid and profound induction of the early growth response (Egr) genes *egr-1* and *egr-3*. In VEGF-treated endothelial cells, induction of Egr-3 was far greater and more prolonged compared with Egr-1. VEGF-mediated stimulation of Egr-3 involved the inducible binding of NFATc, serum response factor, and CREB to their respective consensus motifs in the upstream promoter region of Egr-3. Knockdown of Egr-3 markedly impaired VEGF-mediated proliferation, migration, and tube formation of endothelial cells and blocked VEGF-induced monocyte adhesion. Egr-3 knockdown abrogated VEGF-mediated vascular outgrowth from ex vivo aortic rings and attenuated Matrigel plug vascularization and melanoma tumor growth in vivo. Together, these findings suggest that Egr-3 is a critical determinant of VEGF signaling in activated endothelial cells. Thus, Egr-3 represents a potential therapeutic target in VEGF-mediated vasculopathic diseases. (Blood. 2010;115:2520-2532)

Introduction

The endothelium is a highly malleable cell layer that constantly senses and responds to changes in the extracellular environment. Many extracellular mediators modulate gene transcription in endothelial cells, resulting in such phenotypic changes as cell migration, cell proliferation, angiogenesis, leukocyte adhesion, and hypercoagulability.[1] Tight control of these processes is essential for maintaining homeostasis. Endothelial cell activation, if excessive, oversustained, or spatially and temporally misplaced, may lead to vasculopathic disease such as pathologic angiogenesis, inflammation, and atherosclerosis. Thus, an understanding of the molecular pathways leading to endothelial activation may provide novel insights into therapeutic targets.

Among the nuclear regulators of endothelial cell activation is the early growth response (Egr) family of transcription factors (Egr-1 to Egr-4). These proteins have a highly conserved DNA-binding domain comprising 3 C2H2 zinc finger motifs that recognize a 9-bp DNA consensus element (GCG(G/T)GGGCG). Activation of target gene transcription by Egr family members requires their de novo protein synthesis. Egr-1, the founding member of this family, initially was identified as an immediate early gene in growth factor–treated cells.[2-4] The Egr-3 gene was cloned from a serum-activated cDNA library[5,6] and was originally described as a T-cell receptor–induced cyclosporine A sensitive factor responsible for the up-regulation of FasL.[7] Both Egr-1 and Egr-3 are rapidly induced by extracellular stimuli, and both have been implicated in the proliferation and differentiation of several different cell types, including endothelial cells. Egr-1–null mice display female infertility, whereas Egr-3–null mice demonstrate abnormal neuronal and T-cell development.[6,8,9]

Egr proteins exert overlapping yet distinct functions. Isoform-specific functions may reflect differences in their interactions with coactivators. For example, Egr-1 but not Egr-2/-3 cooperates with NFATc1 in regulating T-cell development.[10] Isoform-specific function also is regulated at the level of feedback inhibition by the NAB family of corepressors (NAB-1 and NAB-2).[11,12] For example, Egr-4 alone is insensitive to inhibition by NAB proteins.[13] Interestingly, in some cases, NAB-2 may function as a coactivator of Egr-1–mediated gene transcription.[14]

Egr-1 has been implicated in several vascular disease states, including ischemia/reperfusion lung injury,[15] atherosclerosis,[16-18] and fibroblast growth factor-2 (FGF-2)–dependent angiogenesis/tumor growth.[19] Although Egr-3 has been studied primarily in the context of lymphocyte and neuromuscular development, recent evidence points to a role for Egr-3 in transducing signals in endothelial cells. For example, we and others[20,21] have shown that Egr-3 is one of the most highly inducible genes in vascular endothelial cell growth factor (VEGF)–treated endothelial cells. Moreover, Egr-3 knockdown attenuated VEGF- and FGF-2–induced growth of cultured endothelial cells.[22]

Here, we show that activation of primary human endothelial cells with VEGF, thrombin, or tumor necrosis factor-α (TNF-α) results in the rapid up-regulation of both Egr-1 and -3. VEGF-mediated induction of Egr-3 is greater and more prolonged compared with Egr-1; involves the inducible binding of NFAT, serum response factor (SRF), and CREB to the Egr-3 proximal

Submitted July 16, 2009; accepted October 24, 2009. Prepublished online as *Blood* First edition paper, November 23, 2009; DOI 10.1182/blood-2009-07-233478.

An Inside *Blood* analysis of this article appears at the front of this issue.

The online version of this article contains a data supplement.

The publication costs of this article were defrayed in part by page charge payment. Therefore, and solely to indicate this fact, this article is hereby marked "advertisement" in accordance with 18 USC section 1734.

promoter; and regulates cell growth, migration, neoangiogenesis, hemostatic balance, and leukocyte adhesion. These findings provide new insights into the molecular basis of endothelial cell activation and suggest that Egr-3 may be therapeutically targeted in states of pathologic angiogenesis and inflammation.

Methods

Cell culture

Human umbilical vein endothelial cells (HUVECs), human coronary artery endothelial cells (HCAECs), human pulmonary artery endothelial cells (HPAECs), human dermal microvascular endothelial cells (HDMVECs), and human skin fibroblasts were purchased from Clonetics. All primary vascular endothelial cells were cultured in EGM-2 MV complete medium (Clonetics). Fibroblasts were culture in Dulbecco modified Eagle medium supplemented with 10% heat-inactivated fetal bovine serum (FBS). Human embryonic kidney (HEK)–293 (ATCC CRL-1573), mouse pancreatic endothelial cells (MS-1; ATCC CRL-2279), mouse Lewis lung carcinoma cells (ATCC CRL-1642), and B16-F10 cells (ATCC CRL-6475) were cultured in Dulbecco modified Eagle medium supplemented with 10% FBS. Human U937 cells (JCRB-9021) were grown in RPMI-1640 medium plus 10% FBS.

ChIP assays

Chromatin immunoprecipitation (ChIP) assays were performed as previously described.[23,24] In brief, sonicated chromatin was immunoprecipitated by the use of antibodies against NFATc1 (Affinity BioReagents), NFATc2 (BD Biosciences), SRF (Santa Cruz Biotechnology), and CREB (Cell Signaling Technology) or normal rabbit/mouse immunoglobulin G (IgG; Sigma-Aldrich), and the precipitates were collected on protein A/G-Sepharose beads (GE Healthcare). Real-time polymerase chain reactions (PCRs) were performed with the primer pairs as shown in supplemental Table 1 (available on the *Blood* website; see the Supplemental Materials link at the top of the online article).

Cell migration assays

Endothelial cells were treated with siRNAs for 24 hours and then serum-starved and labeled with PKH2 dye (Sigma-Aldrich). Migration assays were carried out by the use of the BD Biocoat angiogenesis system (BD Biosciences). Fluorescently labeled cells were seeded on the upper chamber (10^5 cells/250 mL of EBM-2) and incubated with 750 mL of EBM-2 with or without 50 ng/mL VEGF in the lower chamber. After 24 hours, migrated cells were visualized under the fluorescent microscope (Leica [DMIRB]) and quantified by the use of a fluorescence detect-cell image analyzer (Kurabo).

Matrigel plug assay

Growth factor-reduced Matrigel (BD Biosciences) containing 50 ng of VEGF and either 10^9 plaque-forming units (pfu) of Ad-miControl or Ad-miEgr-3 was injected subcutaneously into the flanks of C57BL/6 mice. After 14 days, Matrigel plugs were removed for histologic sections. Alternatively, mice were injected intravenously with 100 μL of 1% Evans blue dye. After 40 minutes, mice were perfused with phosphate-buffered saline containing 2mM EDTA (ethylenediaminetetraacetic acid). Matrigel plugs were removed and incubated with formamide for 2 days to elute Evans blue dye, which was then measured with the use of a spectrophotometer (620 nm). All animal studies involving mice were approved by the Institutional Animal Care and Use Committee at the University of Tokyo.

Aortic ring assay

C57BL/6J mice were injected intravenously with 1.5×10^9 pfu Ad-miControl or Ad-miEgr-3. After 4 days, the descending thoracic aorta was isolated, cut into approximately 1-mm segments, and embedded in Matrigel (BD Biosciences). Aortic rings were incubated with MCDB131 medium (Sigma-Aldrich) plus VEGF or vehicle control in the presence of 10^8 pfu Ad-miControl or Ad-miEgr-3. Culture medium was exchanged every 4 days. Then, 2 weeks later, vessel outgrowth was observed with phase-contrast microscopy. Total tube length was calculated by the use of the image analyzer software from Kurabo.

Monocyte adhesion assay

HUVECs were transfected with siRNAs and seeded on 24-well tissue-culture plates. Cells were grown to confluence, incubated with EBM-2 containing 0.5% FBS for 18 hours, and then treated in the presence or absence of 50 ng/mL VEGF for 6 hours. Cells were then incubated with control IgG or neutralizing antibodies against vascular cell adhesion molecule-1 (VCAM-1) or E-selectin for 30 minutes and overlaid with 3×10^5 PKH-26 (Sigma-Aldrich)–labeled U937 cells (per well). At 90 minutes later, cells were washed with Hanks buffered saline (Invitrogen) and examined with fluorescent microscopy (Leica [DMIRB]). The adhesion intensities were measured with Metamorph (Molecular Devices Corp) and a cell image analyzer (Kurabo).

Solid tumor model

We mixed 10^6 logarithmically growing B16-F10 melanoma cells with 100 μL of Matrigel (BD Biosciences) and implanted subcutaneously into the flank of C57/BL6 mice. When the tumor reached 10 mm^3 in volume, it was injected with 5×10^9 pfu of Ad-miControl or Ad-miEgr-3. Tumor volume (mm^3) was measured by the use of calipers. Additional experimental procedures were shown in the supplemental Methods.

Results

Activation agonists induce Egr-1 and Egr-3 mRNA and protein expression in primary human endothelial cells

We have previously shown that different activation agonists result in overlapping yet distinct patterns of gene expression in endothelial cells.[21,25] To more comprehensively define these patterns, we used DNA microarrays to assay transcriptional profiles in HUVECs treated in the absence or presence of VEGF, thrombin, or TNF-α for 1, 4, and 18 hours. As shown in Figure 1A, the majority of thrombin-responsive genes were up-regulated at 4 hours, whereas VEGF- and TNF-α–responsive genes were most highly represented at 18 hours. The 3 agonists induced the expression of a common set of genes at each time point (Figure 1A). At 1 hour, all such genes were transcription factors/cofactors. The most highly induced of these early-response genes were Egr-1 and Egr-3 (>10-fold).

Quantitative real-time PCR was used to assay time-dependent mRNA expression of Egr-1 and -3 in VEGF-treated endothelial cells. In HUVECs, Egr-1 was maximally induced (32-fold, relative to cyclophilin mRNA) at 30 minutes, whereas Egr-3 mRNA expression peaked at 45 minutes (314-fold; Figure 1B). Similar results were obtained with HCAEC, HPAEC, and HDMVEC (Figure 1B). Western blot analyses demonstrated time-dependent induction of Egr-1 and -3 protein expression in VEGF-treated HUVECs, with maximal levels occurring at 1 and 2 hours, respectively (Figure 1C). Compared with Egr-1, expression of Egr-3 was more sustained, returning to baseline levels only after 12 hours (data not shown). Thus, VEGF results in early transient induction of Egr-1 and more pronounced, delayed, and sustained induction of Egr-3 in primary human endothelial cells.

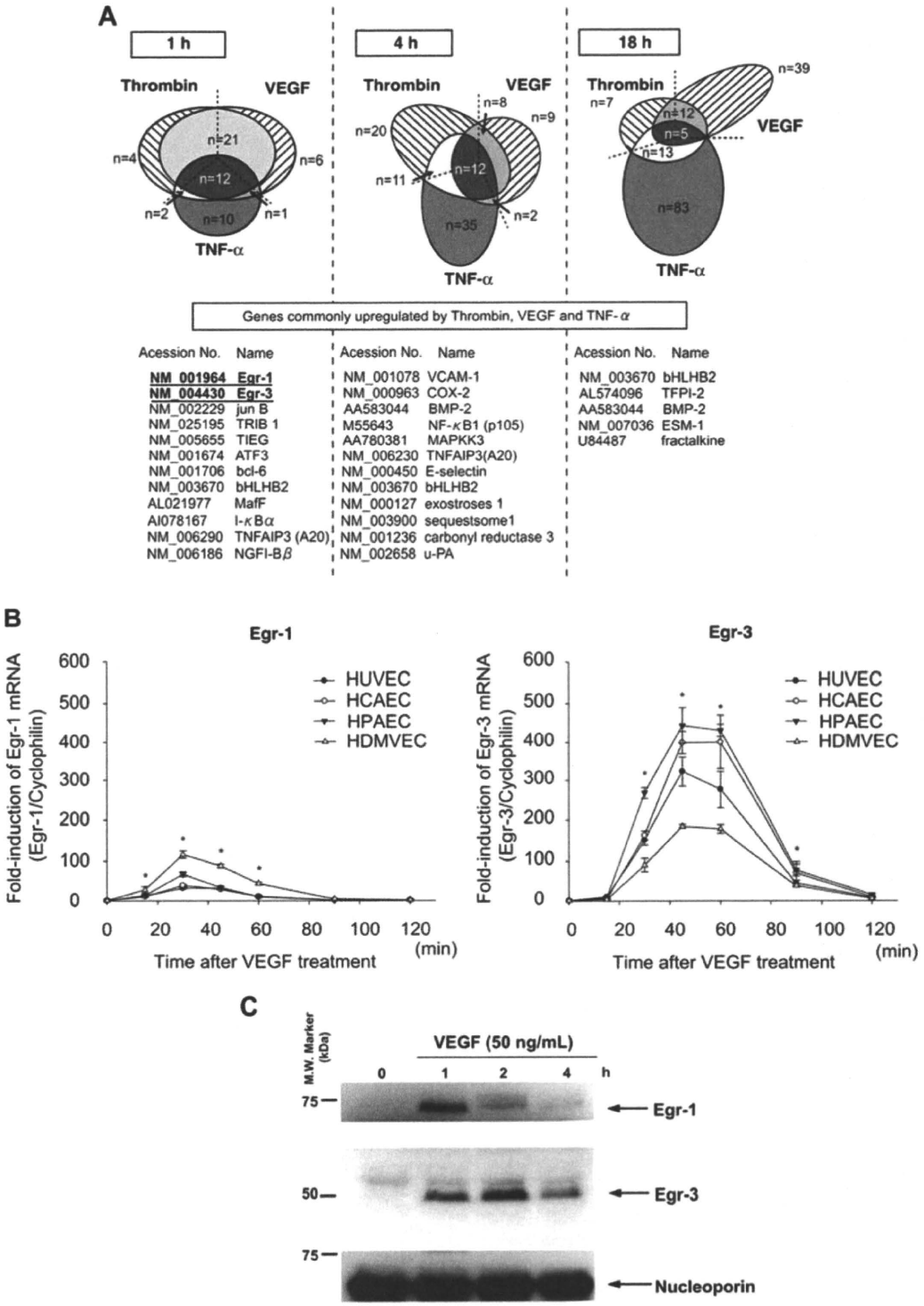

Figure 1. Activation agonists result in rapid, high-level induction of Egr-3 in primary human endothelial cells. (A) DNA microarrays of HUVECs treated with 50 ng/mL VEGF, 2 U/mL thrombin, or 10 ng/mL TNF-α for 1, 4 or 18 hours. Shown is Venn diagram of agonist-induced genes. (B) Real-time PCR time-course analysis of Egr-1 and -3 mRNA expression in VEGF-treated HUVECs, HCAECs, HPAECs, and HDMVECs. *$P < .001$ compared with 0 hours (no treatment) in HUVECs, HCAECs, HPAECs, and HDMVECs. (C) Time-dependent induction of Egr-1 and -3 protein expression in VEGF-stimulated HUVECs. Western blot analysis was performed by the use of antibodies against Egr-1 or -3. Antinucleoporin antibody was used as an internal loading control. The data are representative of 3 independent experiments.

VEGF-mediated induction of Egr-1 and Egr-3 in primary human endothelial cells involves overlapping but distinct signaling pathways

We next wished to determine whether the distinct time course of Egr-1 and -3 induction in VEGF-treated endothelial cells reflected different underlying signal transduction pathways. To that end, real-time PCR was carried out in control and VEGF-treated HUVECs preincubated in the absence or presence of signaling inhibitors. VEGF-mediated expression of Egr-1 and -3 was blocked by neutralizing antibody against VEGFR2/KDR (Table 1). VEGF stimulation of Egr-1 and -3 was similarly attenuated by inhibitors of MEK1/2 (PD98059), c-jun N-terminal kinase (SP600125), and

Table 1. Comparison of the VEGF-mediated Egr-1 and Egr-3 expression signals

Name	Target	*egr-1* mRNA reduction rate ± SD (%)	*egr-3* mRNA reduction rate ± SD (%)
DMSO		0	0
KDR nAb.	KDR	−81 ± 6.4*	−87 ± 5.7*
LY294002	PI3K	(superinduced by 60-fold)	−73 ± 2.4*
PD98059	MEK1/2	−68 ± 2.3*	−78 ± 4.4*
SB203580	p38	(superinduced by 10-fold)	N.E.
Cyclosporine A	Calcineurin	N.E.	−75 ± 3.9*
BAPTA-AM	Ca^{2+}	−87 ± 3.9	−99 ± 0.1*
GF109203X	PKCα, βI, βI, σ, γ, ϵ	−44 ± 1.9†	−99 ± 0.1*
Gö6976	PKCα, βI	−40 ± 5.4†	−99 ± 0.1*
Rottlerin	PKCσ, θ	(superinduced by 10-fold)	−59 ± 3.2*
SP600125	JNK	−95 ± 2.1*	−99 ± 0.1*
H-85	PKA	(superinduced by 6-fold)	−73 ± 9.7*
Cycloheximide	Protein biosynthesis	(superinduced by 120-fold)	(superinduced by 10-fold)

DMCO indicates dimethyl sulfoxide; JNK, c-jun N-terminal kinase; KDR, kinase domain receptor; MEK1/2, MAP kinase/ERK kinase; N.E., no effect; PI3K, phosphoinositide-3 kinase; PKA, protein kinase A; and PKC, protein kinase C.

*Indicates significant reduction.

†indicates mild reduction.

Ca^{2+} influx (BAPTA-AM) but was unaffected by inhibitors of p38 mitogen-activated protein kinase (SB203580) and de novo protein synthesis (cycloheximide). Classical protein kinase C inhibitors (GF109203x and Gö6976) had a more pronounced effect on VEGF-mediated induction of Egr-3 compared with Egr-1. Finally, VEGF stimulation of Egr-3 but not Egr-1 was significantly blunted by inhibitors of phosphoinositide-3 kinase (LY294002), calcineurin/NFATc (cyclosporine A), protein kinase C-δ (rottlerin), and protein kinase A (H-85; Table 1). Thus, VEGF-mediated expression of Egr-1 and -3 in primary human endothelial cells is governed by overlapping yet distinct signal transduction pathways.

VEGF induction of Egr-3 in primary human endothelial cells is mediated by NFATc, SRF, and CREB

To evaluate the transcriptional mechanisms underlying VEGF-mediated induction of Egr-3, we isolated the human Egr-3 promoter and subcloned a fragment spanning the region between −2544 and +80 into the luciferase vector pGL3. The resulting plasmid (Egr-3 (−2544/+80)-luc) was transiently transfected into primary endothelial cells (HUVECs and HDMVECs) or nonendothelial cells (human skin fibroblasts and HEK-293). The cells were serum-starved and treated in the absence or presence of 50 ng/mL VEGF for 4 hours. As shown in Figure 2A, VEGF resulted in 13.8-fold and 5.1-fold induction of induction of promoter activity in HUVECs and HDMVECs, respectively. In contrast, VEGF failed to activate the promoter in fibroblasts or HEK-293 cells. HUVECs were transiently transfected with a series of progressive 5′ deletions of the Egr-3 promoter. Promoters containing 1502-, 1184-, 896-, and 515-bp 5′-flanking sequences retained full VEGF responsiveness (Figure 2B), whereas further deletion to 37 bp resulted in a significant loss of VEGF induction.

The latter findings suggest that the VEGF-responsive element(s) of the Egr-3 promoter is (are) located between −515 and −37. This region contains a tandem NFAT/NF-κB–like site as well as consensus motifs for CRE and SRE (Figure 2C; supplemental Figure 1).[26] To determine whether one or more of these sites plays a functional role in transducing the VEGF signal, we generated Egr-3-luc constructs containing internal deletions or point mutations of these sequences. An internal deletion of a region spanning the tandem NFAT/NF-κB motifs (between −133 and −101) resulted in a 77% reduction in VEGF response (supplemental Figure 1). Consistent with these findings, point mutations of the tandem sites (Egr-3 [−515/+80]-NFATmut-luc) inhibited VEGF induction by greater than 50% (Figure 2C). An internal deletion of the region containing both the SRE and CRE sites (between −102 and −37) resulted in 80% reduction in VEGF response (supplemental Figure 1). A single point mutation of the SRE (Egr-3 (−515/+80)-SREmut-luc) inhibited VEGF induction by 50% (Figure 2C). Combined mutation of the 2 CRE sites (Egr-3 (−515/+80)-CREmut-luc) yielded a 70% decrease in VEGF response (Figure 2C). Finally, disruption of all sites (NFAT/NF-κB, CRE, and SRE) virtually abrogated VEGF-mediated activation of the Egr-3 promoter (Figure 2C; supplemental Figure 1). Thus, the NFAT/NF-κB, SRE, and CRE elements each play a critical role in mediating VEGF stimulation of Egr-3 promoter activity.

To delineate the DNA-binding proteins involved in this response, we carried out electrophoretic mobility shift analysis by the use of nuclear extracts from VEGF-treated HUVECs and radiolabeled probes spanning the SRE, CRE, or NFAT/NF-κB motifs. The SRE probe demonstrated a slowly migrating DNA-protein complex (supplemental Figure 2A lane 2). The complex was abrogated by unlabeled wild-type but not mutant self-competitor (supplemental Figure 2A lanes 3-4). Preincubation of the reaction mixture with antibodies against SRF but not control IgG resulted in a supershift of the DNA-protein complex (supplemental Figure 2A lanes 5-6). Similarly, radiolabeled probes containing the CRE (supplemental Figure 2B) or NFAT/NF-κB motifs (supplemental Figure 2C) also demonstrated slowly migrating DNA-protein complexes, which were inhibited by unlabeled wild-type but not mutant competitor (supplemental Figure 2B-C).

To assess the role for NFATc, CREB, and SRF in mediating VEGF induction of Egr-3 in its native chromatin context, we used ChIP assays. As shown in Figure 2D, VEGF treatment increased binding of NFATc1 (2.9-fold), NFATc2 (3.2-fold), SRF (2.7-fold), and pCREB (2.5-fold) but not control IgG to the proximal Egr-3 promoter. As a negative control, VEGF failed to alter binding of these transcription factors to the endogenous MyoD promoter (data not shown). Together, these findings suggest that VEGF induces binding of NFATc1, NFATc2, SRF, and CREB to the endogenous Egr-3 promoter endothelial cells.

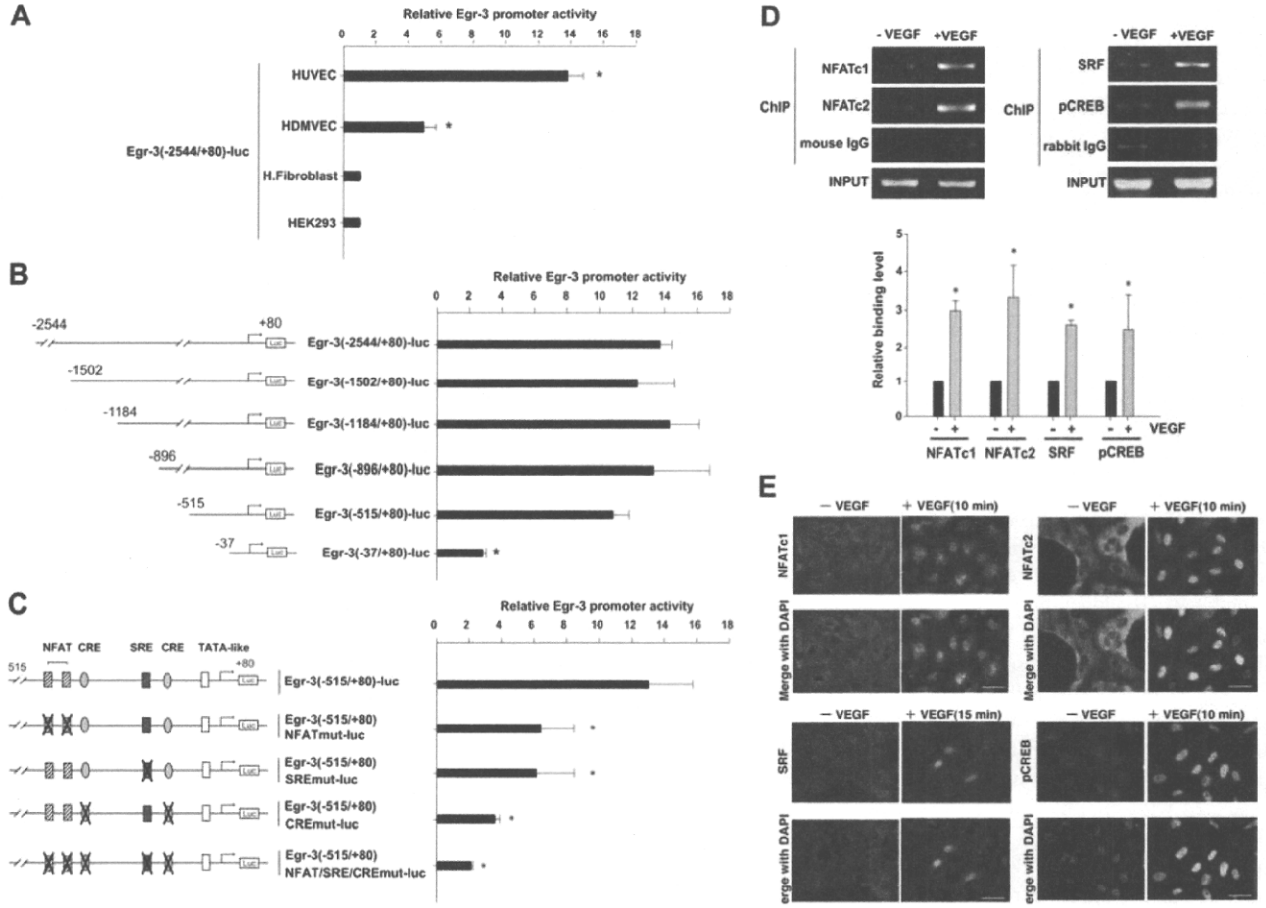

Figure 2. NFAT, SRF, and CREB bind to and transactivate the Egr-3 promoter in primary human endothelial cells. (A) Egr-3 (−2544/+80)-luc was transiently transfected into HUVECs, HDMVECs, human skin fibroblasts (H.Fibroblast), or HEK-293 cells. Cells were treated in the absence or presence of 50 ng/mL VEGF for 4 hours and assayed for reporter gene activity. The results show the mean ± SD of luciferase light units in VEGF-treated cells relative to untreated cells, obtained in triplicate from 3 independent experiments. *$P < .001$ compared with untreated cells. (B) 5′-deletion analysis of Egr-3 promoter activity in control versus VEGF-treated HUVECs. Successive deletions of the 5′-flanking region of Egr-3 were coupled to luciferase in pGL3, and the resulting constructs were transiently transfected into HUVECs. Cells were treated in the absence or presence of 50 ng/mL VEGF for 4 hours and assayed for reporter gene activity. The results show the mean ± SD of luciferase light units in VEGF-treated cells relative to untreated cells obtained in triplicate from 3 independent experiments. *$P < .01$ compared with Egr-3 (−2544/+80)-luc. (C) Analysis of mutant Egr-3 promoter activity in control versus VEGF-treated HUVECs. HUVECs were transiently transfected with either wild-type Egr-3 (−515/+80)-luc or Egr-3 (−515/+80)-luc containing point mutations of NFAT, SRF, and/or CRE motifs; treated in the absence or presence of 50 ng/mL VEGF for 4 hours; and assayed for reporter gene activity. The results show the mean ± SD of luciferase light units in VEGF-treated cells relative to untreated cells obtained in triplicate from 3 independent experiments. *$P < .01$ compared with Egr-3 (−515/+80)-luc. (D) ChIP assays of HUVECs treated in the absence or presence of 50 ng/mL VEGF for 30 minutes. Formalin-fixed chromatin was immunoprecipitated with monoclonal mouse antibodies to NFATc1 or NFATc2 or with mouse control immunoglobulin (IgG; left). Alternatively, formalin-fixed chromatin was immunoprecipitated with rabbit polyclonal antibodies against SRF or phospho-CREB or with rabbit control IgG (right). Precipitated chromatin was PCR amplified (30-35 cycles) and subjected to agarose gel electrophoresis (top). Binding was quantified by the use of real-time PCR (bottom). The results show the mean ± SE of binding level relative to control (without VEGF) obtained from at least 3 independent experiments. *$P < .01$ compared with control. (E) Immunofluorescent studies of NFAT, SRF, and phospho-CREB (pCREB) in control and VEGF-treated HUVECs. Serum-starved cells were incubated in the presence or absence of 50 ng/mL VEGF for the times indicated. The cells were then fixed and incubated with antibodies against NFATc1, NFATc2, SRF, or phospho-CREB, followed by Alexa 488–conjugated second antibody (green). The nuclei were stained with DAPI (blue). Merged images are shown in the bottom row. White bar indicates 20 μm.

To provide additional evidence for the role of these transcription factors in mediating the effect of VEGF on Egr-3 expression, we used immunohistochemistry to localize the proteins of interest in control- and VEGF-treated HUVEC. As shown in Figure 2E, VEGF resulted in marked nuclear localization of NFATc1, NFATc2, and phospho-CREB at 10 minutes and SRF at 15 minutes.

Finally, to test whether NFATc, SRF, and CREB can transactivate the Egr-3 promoter, cotransfection assays were carried by the use of wild-type or mutant Egr-3 luciferase constructs and expression vectors for these transcription factors. Each factor (NFATc, SRF, and CREB) was capable of transactivating the Egr-3 promoter, an effect that was abrogated by mutation of their respective DNA binding sites (supplemental Figure 3). Collectively, promoter-luciferase, electrophoretic mobility shifts, ChIP, and immunohistochemistry assay results strongly implicate a role for NFATc1, NFATc2, SRF, and phospho-CREB in mediating VEGF induction of Egr-3 expression in endothelial cells.

NAB-1 is the predominant NAB isoform in primary human endothelial cells and inhibits Egr-1 but not Egr-3 activity

Svaren et al[12] have implicated a role for NAB-1 and NAB-2 in inhibiting Egr-1 activity. In real-time PCR, HUVECs expressed much greater levels of NAB-1 compared with NAB-2 (supplemental Figure 4A). To determine whether NAB-1 or NAB-2 repress Egr-1 and/or -3 activity, HUVECs were cotransfected with 1 of 2 Egr-responsive promoters (tissue factor or Flt-1) and expression vectors for Egr-1, Egr-3, NAB-1, and/or NAB-2. Egr-1–mediated transactivation of TF and Flt-1 was abrogated both by NAB-1 and NAB-2 (supplemental Figure 4B). In contrast, Egr-3–mediated

transactivation of these 2 promoters was inhibited by NAB-2 alone (supplemental Figure 4B). Cotransfection with plasmids expressing Egr-1, Egr-3, NAB-1, and NAB-2 resulted in comparable expression of their respective genes, as measured by real-time PCR and Western blots (data not shown). Thus, NAB-1 is the predominant NAB isoform in HUVECs and selectively inhibits Egr-1 activity.

Egr-3 knockdown/overexpression in human primary endothelial cells results in altered VEGF-mediated transcriptional profiles

We next wished to analyze the functional relevance of VEGF-inducible Egr-3 in endothelial cells. To that end, we used siRNA to knock down expression of Egr-3. Transient transfection of HUVECs with 2 independent siRNAs against Egr-3 (si-Egr-3 oligo 1 and oligo 2) resulted in significant inhibition of VEGF-responsive Egr-3 mRNA expression (90% and 72% reduction, respectively; Figure 3A) and virtual abrogation of inducible Egr-3 protein expression (Figure 3B). As evidence of specificity, si-Egr-3 failed to inhibit VEGF induction of Egr-1 (supplemental Figure 5). DNA microarrays were carried out in control and Egr-3–deficient HUVECs treated in the absence or presence of 50 ng/mL VEGF. The data were filtered for those genes that were induced greater than 2-fold by VEGF and whose induction was inhibited at least 50% by the 2 independent Egr-3 siRNAs compared with control siRNA (Figure 3C). Among the genes represented were those associated with migration/angiogenesis (eg, CXCL1, SSH1, and ETS-1), coagulation (eg, tissue factor), and inflammation/leukocyte trafficking (eg, VCAM-1 and E-selectin). These changes were validated by the use of quantitative real-time PCR (supplemental Figure 6). These changes were validated by the use of quantitative real-time PCR (supplemental Figure 6). These microarray data have been deposited in the Gene Expression Omnibus (National Center for Biotechnology Information) and are accessible through GEO Series accession number GSE18913.

We next wished to determine whether genes that were affected by Egr-3 knockdown are reciprocally regulated by Egr-3 overexpression. To that end, HUVECs were transduced with doxycycline-regulated adenovirus expressing no cDNA or Egr-3 (Ad-Egr-3). At 2 days after infection, HUVECs were treated in the absence or presence of 1 μg/mL doxycycline for 2 days.

In DNA microarrays, conditional doxycycline-mediated overexpression of Egr-3 resulted in the induction of 24 of the 28 genes that were down-regulated by si-Egr-3 (Figure 3D). Compared with conditional overexpression of Egr-1, Egr-3 induced significantly greater levels of VCAM-1, SSH-1, and CXCL1 (Figure 3D). A comprehensive analysis of the microarray data from Egr-1 versus Egr-3 overexpressing cells revealed a preferential role for Egr-3 in inducing genes related to cell growth and hemostasis (supplemental Figure 7; whole gene lists are shown in supplemental Table 2).

Egr-3 knockdown attenuates VEGF-mediated growth, migration, and tube formation of human primary endothelial cells

On the basis of the Egl-3–mediated transcriptional profiles, we hypothesized that Egr-3 plays a critical role in mediating the phenotypic response of endothelial cells to VEGF, including migration/angiogenesis. To test this hypothesis, HUVECs were transfected with si-Control or si-Egr-3, serum-starved, and treated with or without 50 ng/mL VEGF. Cells were then enumerated over time. VEGF treatment of si-Control–transfected cells resulted in a 2.4-fold increase in cell number after 48 hours (Figure 4A). This effect was inhibited 36% to 75% by Egr-3 knockdown (Figure 4A). There was no evidence of increased apoptosis in si-Egr-3–transfected HUVECs (data not shown).

In modified Boyden chamber assays, VEGF resulted in a 3.6-fold increase in migration of si-Control–transfected HUVEC (Figure 4B). In contrast, VEGF failed to induce the migration of Egr-3 siRNA-treated HUVECs (Figure 4B). Similarly, Egr-3 knockdown inhibited cell migration in a 24-hour cell scratch assay (Figure 4C). VEGF treatment of si-Control–transfected HUVECs induced the formation of tube-like structures in 3-dimensional collagen gels (Figure 4D). This effect was markedly inhibited by each of the 2 siRNAs against Egr-3 (96% or 92% of basal level, respectively; Figure 4D). Collectively, these findings suggest that Egr-3 may play a role in mediating the effect of VEGF on new blood vessel formation.

Egr-3 knockdown attenuates VEGF-mediated monocyte adhesion and tissue factor activity in cultured endothelial cells

The DNA microarrays shown in Figure 3 support a role for Egr-3 in mediating VEGF induction of cell adhesion molecules. To determine whether this effect is functionally relevant, we carried out cell adhesion assays using U937 monocytic cells and HUVECs. VEGF treatment of si-Control–transfected HUVECs resulted in 4.1-fold increased monocyte adhesion. In contrast, VEGF had no effect on U937 cell adhesion to Egr-3–deficient HUVECs (Figure 5A). VEGF-mediated induction of E-selectin and VCAM-1 expression was strongly attenuated by Egr-3 knockdown (Figure 3C; supplemental Figure 6). VEGF-mediated U937 monocyte adhesion was inhibited 64% and 95% in the presence of neutralizing antibody against E-selectin and VCAM-1, respectively (Figure 5B). Egr-3 was also found to mediate VEGF induction of tissue factor (Figure 3C; supplemental Figure 6). Consistent with these findings, Egr-3 knockdown blocked VEGF-mediated tissue factor–dependent activation of factor X (data not shown). Together, these findings suggest that Egr-3 plays a critical role in VEGF-mediated E-selectin/VCAM-1–dependent leukocyte adhesion and tissue factor activity in endothelial cells.

Egr-3 knockdown impairs VEGF-dependent vascular sprouting in aortic ring assays and neovascularization of in vivo Matrigel plugs

Having established a critical role for Egr-3 in VEGF-mediated proliferation and migration of cultured endothelial cells, we wished to evaluate the functional relevance of these findings in vivo. First, we generated adenovirus expressing microRNA against murine Egr-3 (Ad-miEgr-3). Infection of mouse pancreatic microvascular cells (MS-1) with Ad-miEgr-3 resulted in greater than 80% knockdown of VEGF-inducible Egr-3 mRNA expression (Figure 6A). Adenoviral gene delivery was then used to knock down Egr-3 expression in an aortic ring assay. To that end, mice were systemically administered Ad-miControl or Ad-miEgr-3. Aortas were removed 3 days later and plated in Matrigel in the presence or absence of VEGF plus Ad-miControl or Ad-miEgr-3. As shown in Figure 6B, VEGF induced sprouting of new vessels from Ad-miControl–treated aortas (18-fold increase in total tube length). In contrast, VEGF failed to simulate sprouting from Ad-miEgr-3–treated aortas (Figure 6B).